

KIT SCIENTIFIC REPORTS 7635

Radionuclide Source Term for Irradiated Fuel from Prototype, Research and Education Reactors, for Waste Forms with Negligible Heat Generation and for Uranium Tails

Bernhard Kienzler, Marcus Altmaier,
Christiane Bube, Volker Metz

Bernhard Kienzler, Marcus Altmaier, Christiane Bube, Volker Metz

Radionuclide Source Term for Irradiated Fuel from Prototype, Research and Education Reactors, for Waste Forms with Negligible Heat Generation and for Uranium Tails

Karlsruhe Institute of Technology
KIT SCIENTIFIC REPORTS 7635

Radionuclide Source Term for Irradiated Fuel from Prototype, Research and Education Reactors, for Waste Forms with Negligible Heat Generation and for Uranium Tails

Bernhard Kienzler
Marcus Altmaier
Christiane Bube
Volker Metz

Report-Nr. KIT-SR 7635

Dieser Bericht wurde von KIT-INE gemäß Angebot Nr. 20003729 vom 26.07.2011 im Auftrag der Gesellschaft für Anlagen- und Reaktorsicherheit (GRS) mbH, Schwertnergasse 1, 50667 Köln im Rahmen des Projekts „Vorläufige Sicherheitsanalyse Gorleben“ (VSG) erstellt. Der Bericht gibt die Auffassung und Meinung des Auftragnehmers wieder und muss nicht mit der Meinung des Auftraggebers übereinstimmen. Der Bericht wurde unter der Bezeichnung KIT-INE 001/12 an den Auftraggeber (GRS) übergeben.

Impressum

Karlsruher Institut für Technologie (KIT)
KIT Scientific Publishing
Straße am Forum 2
D-76131 Karlsruhe
www.ksp.kit.edu

KIT – Universität des Landes Baden-Württemberg und
nationales Forschungszentrum in der Helmholtz-Gemeinschaft



Diese Veröffentlichung ist im Internet unter folgender Creative Commons-Lizenz
publiziert: <http://creativecommons.org/licenses/by-nc-nd/3.0/de/>

KIT Scientific Publishing 2013
Print on Demand

ISBN 978-3-86644-964-0

Radionuclide Source Term for Irradiated Fuel from Prototype, Research and Education Reactors, for Waste Forms with Negligible Heat Generation and for Uranium Tails

Abstract

Within the project "Provisional Safety Analysis for Gorleben (vSG)", the source terms for a series of waste forms have been derived. This report comprises the source terms for fuel elements from the pilot reactors AVR/THTR, from the research reactors KNK II and NS Otto Hahn, and from the research and material test reactors BER II and FRM II. Further, graphite wastes, compacted structural materials from conditioning of spent LWR fuel elements, the tails from uranium enrichment and other wastes with negligible heat generation are considered. The other wastes with negligible heat generation comprise cemented waste forms and wastes solidified in bitumen and plastic materials. For these materials, the characteristic physical and chemical properties, element and radionuclide inventory, and the kinetics of radionuclide release are described. The boundary conditions are discussed for several disposal concepts developed within the project: A - emplacement of wastes with negligible heat generation, B1 and B2 - emplacement in horizontal galleries, and C - emplacement in vertical boreholes. The boundary conditions include the evolution of the geochemical conditions, the generation of a H₂ atmosphere in LLW emplacement rooms in the presence of steel containers as well as microbial degradation processes. The geochemical performance of containers of the Konrad type IV and type VI is evaluated including self-shielded concrete and steel containers.

The source term includes the kinetics of radionuclide release and the maximum radionuclide concentrations in the different emplacement rooms under the expected geochemical boundary conditions. The maximum radionuclide concentrations are assessed based on the concept of thermodynamic solubilities assuming that concentrations are limited by solubility-controlling solids only. Solubility-controlled element concentrations in NaCl, MgCl₂ and CaCl₂-rich brines are provided for Am(III), Th(IV), U(IV), Np(IV), Pu(III), Pu(IV), Tc(IV) and for Zr(IV). Finally, sorption of radionuclides onto zircaloy compounds, iron phases, corroded cement products and rock salt is described. Open questions and recommendations are derived resulting from the compilation of the relevant data and processes of the various waste forms.

Radionuklid-Quellterm für bestrahlten Kernbrennstoff aus Prototyp-, Forschungs- und Schulungsreaktoren, für Abfälle mit vernachlässigbarer Wärmeentwicklung und für Uran Tails.

Zusammenfassung

Im Projekt "Vorläufige Sicherheitsanalyse Gorleben (vSG)" wurden Quellterme für verschiedene Abfälle abgeleitet. Diese umfassen abgebrannte Brennelemente der Prototypreaktoren AVR und THTR, sowie KNK II und dem Nuklearschiff NS Otto Hahn, von den Forschungs- und Materialtestreaktoren BER II und FRM II. Weiterhin wurden graphithaltige Abfälle, kompaktierte Strukturmaterialien aus der Pilotkonditionierungsanlage für abgebrannte Brennelemente aus Leichtwasserreaktoren, Tails aus der Urananreicherung und sonstige Abfälle mit vernachlässigbarer Wärmeentwicklung betrachtet. Die sonstigen Abfälle mit vernachlässigbarer Wärmeentwicklung beinhalten u. a. zementierte Abfälle und in Bitumen bzw. Plastikmaterialien verfestigte Abfälle. Für alle diese Abfallarten wurden die charakteristischen physikalischen und chemischen Eigenschaften, Element- und Radionuklidinventare, sowie die Kinetiken der Radionuklidfreisetzung beschrieben. Die zugrunde gelegten Randbedingungen wurden für die verschiedenen im Projekt betrachteten Einlagerungsvarianten diskutiert. Dies beinhaltet die Variante A – Einlagerung von Abfällen mit vernachlässigbarer Wärmeentwicklung, B1 und B2 – Einlagerung in horizontale Strecken und C – Einlagerung in vertikale Bohrlöcher. Die Randbedingungen schließen die Entwicklung der geochemischen Bedingungen, die Entwicklung der H₂ Atmosphäre in den Einlagerungskammern bei Anwesenheit von Stahlbehältern und die mikrobielle Degradationsprozesse mit ein. Das Verhalten der Konrad Behälter Typ IV und Typ VI wird einschließlich der selbstabschirmenden Beton- und Stahlbehälter bewertet.

Der Quellterm beinhaltet die Kinetik der Radionuklidfreisetzung und die maximalen Radionuklidkonzentrationen in den verschiedenen Einlagerungskammern unter den erwarteten geochemischen Umgebungsbedingungen. Hierbei wird auf das Konzept der thermodynamischen Löslichkeit von Radionukliden zurückgegriffen und reine Löslichkeitslimitierung der Radionuklidkonzentrationen unterstellt. Maximale (löslichkeitsbegrenzte) Radionuklidkonzentrationen werden für Am(III), Th(IV), U(IV), Np(IV), Pu(III), Pu(IV), Tc(IV) und Zr(IV) in NaCl, MgCl₂ und CaCl₂ reichen Lösungen bei hohem pH abgeleitet. Schließlich werden Sorptionsdaten von Radionukliden auf Zircaloy Verbindungen, Eisenphasen, korrodierten Zementprodukten und auf Steinsalz angegeben. Offene Fragen und Empfehlungen werden formuliert, die aus der Zusammenstellung der relevanten Daten und Prozesse der verschiedenen Abfälle resultieren.

TABLE OF CONTENTS

1	Introduction.....	1
2	Relevant data and Processes.....	3
2.1	Fuel elements from the AVR/THTR.....	3
2.1.1	Characteristic Physical Properties of BISO and TRISO graphite.....	4
2.1.2	Characteristic Chemical Properties of BISO and TRISO graphite.....	5
2.1.3	Element and Radionuclide Inventory of AVR/THTR fuel elements	6
2.1.4	Kinetics of Radionuclide Release from AVR/THTR fuel elements	6
2.2	Fuel elements from the KNK II and the MS Otto Hahn.....	9
2.2.1	Characteristic Properties of KNK II spent fuel	9
2.2.2	Characteristic Properties of NS Otto Hahn spent fuel.....	10
2.2.3	Element and Radionuclide Inventory of NS Otto Hahn spent fuel.....	11
2.2.4	Kinetics of Radionuclide Release of NS Otto Hahn spent fuel.....	12
2.3	Fuel elements from the research reactors BER II and FRM II	12
2.3.1	Characteristic Properties of FRM II.....	13
2.3.2	Characteristic Properties of BER 2 fuel.....	14
2.3.3	Element and Radionuclide Inventory	14
2.3.4	Kinetics of Radionuclide Release	14
2.4	Graphite Wastes	15
2.4.1	Characteristic Properties of Graphite Wastes.....	15
2.4.2	Element and Radionuclide Inventory in graphite wastes.....	16
2.4.3	Kinetics of Radionuclide Release from graphite wastes.....	16
2.5	Compacted structural materials from conditioning of spent LWR fuel elements.....	17
2.5.1	Characteristic Properties of compacted structural material.....	18
2.5.2	Element and Radionuclide Inventory of compacted structural material.....	18
2.5.3	Kinetics of Radionuclide Release	19
2.6	Tails from uranium enrichment	19
2.6.1	Characteristic Properties of tails from uranium enrichment	19
2.6.2	Element and Radionuclide Inventory	20
2.6.3	Kinetics of Radionuclide Release	20
2.7	Other mixed wastes with negligible heat generation.....	20
2.7.1	Characteristic properties of the mixed wastes.....	20
2.7.2	Element and Radionuclide inventory	20
2.7.3	Kinetics of radionuclide release from other mixed wastes.....	21
2.8	Cemented waste forms.....	21
2.8.1	Characteristic properties of cemented waste forms.....	22
2.8.2	Element and Radionuclide Inventory	23
2.8.3	Kinetics of Radionuclide Release	24

2.9	Wastes solidified in bitumen and plastic materials	26
3	Boundary Conditions for the source term	27
3.1	Disposal concept	27
3.1.1	A – emplacement of wastes with negligible heat generation	27
3.1.2	B1 and B2 - emplacement in horizontal galleries.....	29
3.1.3	C - emplacement in vertical boreholes.....	31
3.2	Evolution of the geochemical conditions.....	32
3.3	Generation of H ₂ in a LLW emplacement chamber in the presence of steel containers	35
3.4	Chemical degradation processes	36
3.5	Biodegradation processes.....	36
4	Performance of containers	39
4.1	Self-shielding concrete waste containers	39
4.2	Steel containers	41
5	Source Term.....	43
5.1	Kinetics of radionuclide release.....	43
5.2	Maximum radionuclide concentrations in the emplacement rooms.....	44
5.3	Effect of organic complexing agents.....	48
6	Sorption	51
6.1	Sorption onto zircaloy compounds.....	51
6.2	Sorption onto iron phases.....	51
6.3	Sorption onto corroded cement products.....	52
6.4	Sorption onto rock salt.....	53
7	Open Questions and Recommendations.....	55
8	References	57
Annex A	Abbreviations	65

LIST OF TABLES

Tab. 1	Fuel elements used in the AVR until 1989 [9]	4
Tab. 2	AVR spent fuel elements investigated by Zhang [16]	7
Tab. 3	Measured radionuclide inventory in the AVR spent fuel elements investigated by Zhang [16]	7
Tab. 4	Characteristics of irradiated fuel samples after dissolution in 7-10 n HNO ₃ (Kleykamp [22])	10
Tab. 5	Characteristic data of the reactor of the NS OTTO HAHN [23]	10
Tab. 6	Comparison between measured and calculated fuel elements in KNK II [26].....	11
Tab. 7	Characteristic data of the BER-2 reactor according to Axmann and Didier [29].....	14
Tab. 8	Characteristic data of the graphite wastes [3]	16
Tab. 9	Radionuclide inventory in the graphite-containing wastes [3]	16
Tab. 10	Inventory of the compacted structural materials including waste package [3].	18
Tab. 11	Inventory of uranium tails including waste package [3].	20
Tab. 12	Total inventory of the mixed wastes with negligible heat generation [3].	21
Tab. 13	Fitted apparent D_a and diffusion coefficients of water D_w , D_{exp} obtained from small-scale laboratory tests and retention ratio D_a/D_w . Data taken from [55], if not indicated. ..	25
Tab. 14	Leach rates of NaNO ₃ containing bitumen waste forms [66].....	26
Tab. 15	Leach rates in water for spent ion exchange resins solidified in various matrices [67]	26
Tab. 16	Dimensions of Konrad containers (box-type) for waste with negligible heat generation [4].	27
Tab. 17	Characteristics of the disposal concept for the uranium tails [3, 4]	28
Tab. 18	Characteristics of the disposal concept for other mixed wastes [3, 4]	28
Tab. 19	Characteristics of the disposal concept for the graphite wastes [3, 4]	29
Tab. 20	Dimensions of CASTOR containers for waste of prototype and research reactors [4].	30
Tab. 21	Container concept for wastes from research and prototype reactors [4].	30
Tab. 22	Dimensions of BSK casks for waste of prototype and research reactors [4]	31
Tab. 23	Characteristic data of some emplacement rooms for specific wastes	33
Tab. 24	Corrosion of nodular graphite steel GGG 40.3 and fine grained steels as function of the temperature in MgCl ₂ -rich and saturated NaCl solution (after Smailos et al. [71-75]).	35
Tab. 25	Degradation and CO ₂ formation by microbial degradation of cellulose [81].....	37
Tab. 26	Degradation rate and CO ₂ formation rate by microbial degradation of bitumen [64, 82] ..	37
Tab. 27	Initial composition of the concrete.	40
Tab. 28	Changes in the composition of the concrete after ~11 years storage in MgCl ₂ brine	40
Tab. 29	Percentage of rapid (instant) radionuclide release from NS OTTO HAHN fuel assuming a heavily disturbed UO ₂ matrix.	43

Tab. 30	Geochemical conditions of NaCl, MgCl ₂ and CaCl ₂ solution and dominating radionuclide oxidation states expected in the emplacement rooms containing the wastes with negligible heat generation.	45
Tab. 31	Solubility controlled upper-limit concentrations in NaCl, MgCl ₂ and CaCl ₂ solution for the emplacement rooms of wastes with negligible heat generation	47
Tab. 32	Overview on sorption experiments for radionuclides onto iron phases	52
Tab. 33	Sorption coefficients (Rs) in the cement/MgCl ₂ brine system after about 9 months.....	52
Tab. 34	Americium and Plutonium retention in high pH and Ca ²⁺ systems [88]	53
Tab. 35	Sorption coefficients (Rs) in the systems rock salt (ERAM) / MgCl ₂ and NaCl solution [95]	53

LIST OF FIGURES

Fig. 1	Schematic configuration of fuel pebbles, TRISO spheres and fuel kernels (modified after [5])	3
Fig. 2	Cross sections of BISO and TRISO particles [18].....	8
Fig. 3	Fractional release of ^{137}Cs inventory in Q-Brine at 90 °C and 13 MPa [14].....	9
Fig. 4	Fuel element consisting of 113 involute fuel plates (according to TUM FRM II Homepage [28]). The control rod, which moves inside the fuel element, is not shown.	13
Fig. 5	Schematic illustration showing the structural parts of a BWR Siemens ATRIUM 9x9 fuel assembly [41]	17
Fig. 6	Observed Cs release from simulated full-scale cemented waste forms [56].....	24
Fig. 7	Observed uranium release from simulated full-scale cemented waste forms [56].....	25
Fig. 8	West field section of the planned repository building (according to the optimized disposal concept of Bollingerfehr [69]).	29
Fig. 9	East field of the planned repository building where wastes from research reactors are planned to be stored (according to disposal concept B1 [4])	30
Fig. 10	East field of the planned repository building, where wastes from research reactors are planned to be stored (according to disposal concept C [69])	32
Fig. 11	Evolution of pH_m and major cations in initially MgCl_2 -rich solutions upon reaction with cement product. Lines represent simulated results, symbols represent results from experiments at laboratory-scale in the case of $\xi < 1.1$ and with full-scale cemented waste simulates in the case of $\xi = 3.0$	34
Fig. 12	Evolution of pH_m and major cations in initially NaCl -rich solution upon reaction with cement product. Lines represent simulated results, symbols represent results from experiments with full-scale cemented waste simulates at $\xi = 2.8$	34
Fig. 13	Schematic illustration of MOSAIK [®] II canister for disposal of evaporator concentrates and ionic exchanger resins (image provided by GNS)	35
Fig. 14	Cut through a cylindrical self-shielded concrete disposal container after corrosion in saturated MgCl_2 solution (Q brine) for 11 yrs.	40
Fig. 15	Chloride diffusion coefficients in cement at different degrees of water saturation [83]. ...	41
Fig. 16	Solubility of $\text{ZrO}_2 \cdot x\text{H}_2\text{O}(s)$ in NaClO_4 , NaCl , and CaCl_2 solutions at 20-25 °C [90].	46
Fig. 17	Solubility of $\text{ThO}_2 \cdot x\text{H}_2\text{O}(s)$ in NaClO_4 , NaCl , and CaCl_2 solutions at 17-25 °C [90].	46
Fig. 18	Solubility of $\text{PuO}_2 \cdot x\text{H}_2\text{O}(s)$ in MgCl_2 and CaCl_2 solutions [92].	46
Fig. 19	Solubility of $\text{NpO}_2 \cdot x\text{H}_2\text{O}(s)$ in CaCl_2 solutions [93].	46
Fig. 20	Comparison of tetravalent actinide solubility in CaCl_2 solution [93].	46
Fig. 21	Speciation diagram of Am in NaCl solution in the presence of CO_3 and SO_4 according to data given in Tab. 30.	48
Fig. 22	Effect of pH on the sorption behavior of Sr onto hydrous ZrO_2 [100].	51
Fig. 23	Effect of pH on the sorption behavior of Cs onto hydrous ZrO_2 [99] (at pH = 10: 20 % adsorption)	51

1 Introduction

In the scope of the preliminary safety analysis for Gorleben (vSG), KIT-INE prepared a report on the source term for HLW glass, spent nuclear fuel, and compacted hulls and end pieces (CSD-C waste) [1]. The expected geochemical conditions were derived for the source term, kinetically and thermodynamically controlled radionuclide mobilization processes were discussed as well as the influence of the temperature on the different processes. The geochemical scenario for the heat-generating wastes was based on the presence of NaCl or MgCl₂-rich solutions. Maximum concentrations of the radionuclides Am, Th, U, Np, Pu, Tc, Zr, Se and rare earth elements were provided based on concentrations determined by the solubility of corresponding solid phases. Radionuclide retention by sorption processes was assigned a minor relevance within the planned backfill concept using crushed rock salt as backfill material.

In contrast to the ideas developed during the AKEnd discussions in 2000 [2], the concept for nuclear waste disposal in the Gorleben salt dome considers disposal not only of HLW and spent nuclear fuel from power reactors, but also of a series of wastes with negligible heat generation. For this reason, the source term for radionuclide release needs to be complemented to account for the following radioactive wastes [3]:

- Irradiated fuel from prototype, research and education reactors
 - Spherical fuel elements from the AVR/THTR
 - Fuel elements from the KNK II and the MS Otto Hahn
 - Fuel elements from the research reactors FRM II, BER II and FRMZ
- Waste forms with negligible heat generation and uranium tails
 - Graphite wastes
 - Compacted structural materials from conditioning of spent fuel elements from LWRs
 - Tails remaining from production of enriched uranium for fuel elements (for disposal, it is planned to transform the tails into U₃O₈; the tails may additionally contain resins, some 2 % uranium fluoride UO₂F₂ as well as unreacted hydrofluoric acid (HF) at an unknown concentration)
 - Other waste forms with negligible heat generation, such as cemented waste forms in steel sheet or cast steel canisters or in self-shielding concrete casks (these wastes contain steel and various other components such as concrete, cement, lead, resins, plastics, bitumen, cellulose, EDTA and other complexing agents, as well as tensides and other organic and inorganic carbon compounds)

The radionuclide mobilization for these waste forms will be described on the present state-of-the-art of science and technology. This includes describing the geochemical conditions in the near-field of these wastes in contact with NaCl and MgCl₂ rich solutions by means of geochemical model calculations. The different disposal and backfill concepts A, B1, B2 and C [4] will be considered. The kinetics controlling the corrosion of cementitious materials both for waste forms and for self-shielding concrete containers will be described and the radionuclide concentrations as function of the disposal

concept and the evolution of the geochemical environment will be elaborated. Furthermore, the chemical interactions of complexing waste components with radionuclides will be discussed.

2 Relevant data and Processes

2.1 Fuel elements from the AVR/THTR

The development of high temperature reactor (HTR) fuels in Germany was systematically performed in the 1970's and the 1980's. During this time, NUKEM successfully manufactured more than one million fuel elements for the HTR reactor of the "Arbeitsgemeinschaft Versuchsreaktor GmbH" (AVR) at Jülich and for the "Thorium-Hochtemperaturreaktor" (THTR) at Hamm-Uentrop in Germany.

The HTR fuel consists of small fuel kernels of about 200 - 500 μm in diameter. Each of these uranium oxide or carbide kernels is coated with several layers of pyrocarbon (PyC). TRISO particles, which were used since ~1985, are characterized by an additional silicon carbide layer (cf. Fig. 1). While the inner pyrocarbon layer is porous and capable to absorb gaseous fission products, the dense outer PyC layer forms the barrier against fission product release. The SiC layer improves the mechanical strengths of this barrier and thus the retention capacity for certain fission products. The approximately 10 % enriched uranium TRISO coated particles are contained in a moulded graphite sphere. A fuel sphere consists of approximately 9 g of uranium (some 15000 particles) and has a diameter of 60 mm; the total mass of a fuel sphere is 210 g [5].

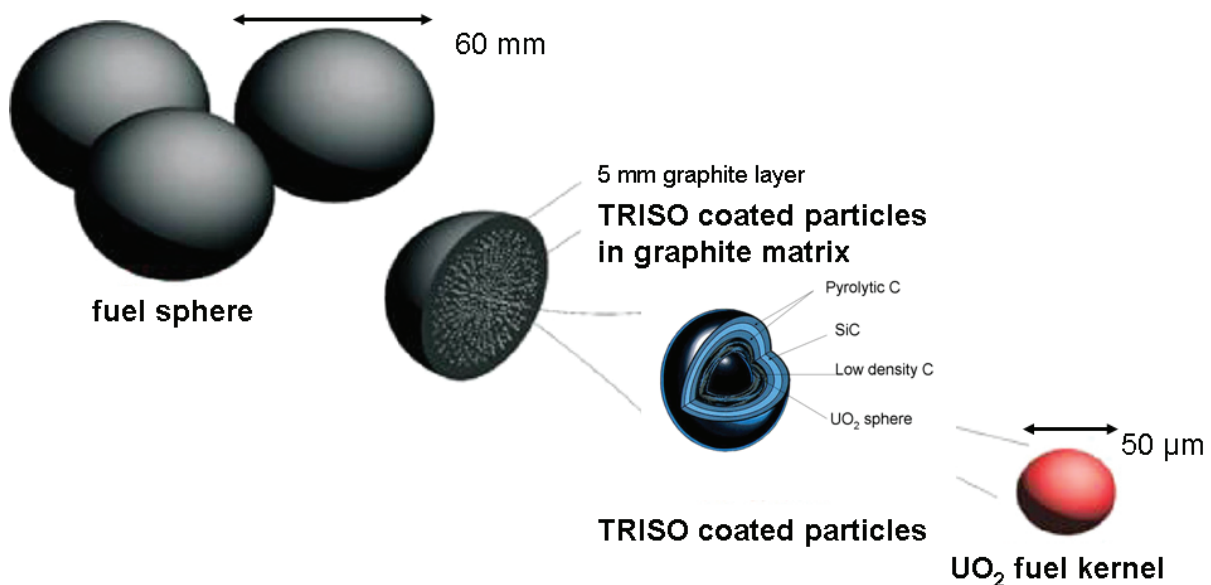


Fig. 1 Schematic configuration of fuel pebbles, TRISO spheres and fuel kernels (modified after [5])

The average burnup of the THTR reactor in Germany amounted to $\sim 85 \text{ GWd}/t_{\text{HM}}$, i.e. up to almost 8.8 % FIMA (fissions per initial metal atom) [6]. For comparison, a typical LWR burnup is in the range of $\sim 50 \text{ GWd}/t_{\text{HM}}$, corresponding to a FIMA of $\sim 5.5 \%$.

During operation of the AVR, several steps of the fuel development were tested. In summary, the various cores of AVR comprised the following fuel elements:

The first AVR core consisted of U-Th mixed carbide particles, produced by Union Carbide, USA. These fuel elements were hollow spheres of graphite ($\varnothing 60 \text{ mm}$) where the inner void ($\varnothing 40 \text{ mm}$) was filled with a mixture of coated particle of 0.3 mm diameter and graphite. The uranium/thorium ratio

was 1:5. The fuel particles were coated by a buffer layer of carbon compensating for the swelling of the fuel under irradiation and a pyro carbon layer providing for gas tightness (BISO). Further types of fuel elements have been used: "Wall paper" type U-Th mixed carbide particles fuel elements, homogeneously distributed U-Th mixed carbide and U-Th oxide particles fuel elements and U-Th oxide with TRISO coating [7, 8]. 14 different types of fuel elements were used in the AVR [9]. The burnup of the AVR reactor in Jülich was in the range between 9.34 and 11.07 % FIMA [9, 10].

Tab. 1 Fuel elements used in the AVR until 1989 [9]

Type of fuel element	Fuel	Coating	Composition of the fuel per fuel element / g			Number of fuel elements in the AVR*
			²³⁵ U	U _{tot}	Th	
First core	(U,Th)C ₂	HTI-BISO	1.00	1.08	5.00	30155
Wall paper fuel elements	(U,Th)C ₂	HTI-BISO	1.00	1.07	5.00	7504
Isostatic pressed graphite elements						
carbide	(U,Th)C ₂	HTI-BISO	1.00	1.08	5.00	50840
Isostatic pressed graphite elements						
oxide	(U,Th)O ₂	HTI-BISO	1.00	1.08	5.00	72418
THTR fuel elements	(U,Th)O ₂	LTI-BISO	1.00	1.08	5.00	6083
	(U,Th)O ₂	HTI-BISO	0.96	1.03	10.20	35415
	UO ₂ , ThO ₂					
	UO ₂ , ThO ₂	LTI-BISO	1.00	1.08	10.00	1440
	UC ₂ , ThO ₂	LTI-BISO	1.00	1.08	10.00	1610
	UC ₂ , ThO ₂	LTI-BISO	1.00	1.08	5.00	6067
Separated burnup and breeding particles	UCO,	LTI-BISO	1.00	1.08	5.00	5860
	ThO ₂	LTI-BISO	1.00	1.08	5.00	5363
	UO ₂	LTI-BISO	1.40	6.00	0	2400
	UO ₂	LTI-TRISO	1.00	10.00	0	24611
oxides at low enrichment	UO ₂	LTI-TRISO	1.00	20.00	0	29090

* 9305 of the 288161 AVR fuel elements are not listed in the table; information on their composition is missing

The inventory of radionuclides to be disposed of from AVR operation is generated from irradiation of 433.026 kg ²³⁵U, 1008.986 kg ²³⁸U and 2116.881 kg ²³²Th. The amount of fission products is given in [3].

In total, 288161 AVR and 611878 HTHR fuel elements have to be disposed of in Germany [4, 11]. These fuel elements are stored in dry storage cans (AVR-TLK) containing 950 fuel elements, each. Two AVR-TLKs are planned to be stored in each CASTOR THTR/AVR. According to the disposal concept of working package AP 5 [4], 152 CASTOR THTR/AVR will be needed for the storage of AVR fuel elements and another 305 for the fuel elements of the THTR.

2.1.1 Characteristic Physical Properties of BISO and TRISO graphite

The details on characteristic physical and chemical properties of graphite used for AVR and THTR fuel elements which are described in chapters 2.1.1 and 2.1.2 are mainly taken from an IAEA document

“Characterization, Treatment and Conditioning of Radioactive Graphite from Decommissioning of Nuclear Reactors. TECDOC 1521, 2006” [12].

Fast neutron irradiation and radiolytic oxidation may radically change the physical and mechanical properties of nuclear graphite. In the high temperature helium cooled reactor, where the graphite is operated in an inert atmosphere, radiolytic oxidation is not an issue and the component’s shape and size will not be greatly affected during the operational life.

Radiolytic oxidation of graphite could only occur when the storage / disposal canisters are corroded and contact between an oxid atmosphere and the graphite would be possible. A contact with an oxid atmosphere is not likely under disposal conditions, since oxygen will be preferentially consumed by the corrosion of steel.

Wigner energy (or “stored” energy) is generated in graphite under neutron irradiation because carbon atoms are displaced from their normal lattice positions into configurations of higher potential energy [8]. The quantity of accumulated “stored” energy is a function of fast neutron flux, irradiation time, and temperature. The higher the irradiation temperature, the lower is the amount of “stored” energy. In all cases, a saturation point may be achieved in terms of the total amount of stored energy for long periods of irradiation. The maximum amount of stored energy ever found in a graphite sample is ~2700 J/g, which if all released at once could theoretically lead to a temperature rise of several hundred degrees assuming adiabatic conditions.

The stored Wigner energy can be released if the graphite is heated above its irradiation temperature (50K above is typical to achieve a significant release rate), although temperatures above 2000 °C are required to release all the stored energy.

Stored (Wigner) energy is not an issue in HTR because of the very high temperatures of the graphite during operation. Since all temperatures under disposal conditions will be below 200 °C, stored energy - if present - will not be released instantaneously.

During reactor operation the graphite components (incl. TRISO/BISO) can change dimensions and this can lead, in some cases, to considerable deformations. Graphite components are polycrystalline in nature and changes in their physical irradiation properties are dominated by irradiation-induced changes to the graphite crystallites.

The dimensional change is not relevant under disposal conditions, since irradiation is negligible.

In deep geological disposal, the thermal conductivity of the graphite waste controls the maximum temperature within the storage casks. Due to the fast neutron irradiation, the thermal conductivity of graphite is in the range 2 to 3 W m⁻¹ K⁻¹. Non-irradiated graphite shows values of around 100 - 200 W m⁻¹ K⁻¹.

2.1.2 Characteristic Chemical Properties of BISO and TRISO graphite

Graphite is a material of low chemical reactivity and generally benign properties. Chemical reaction in graphite takes place only with extremely reactive reagents. The oxidation reaction in air was comprehensively reviewed [12]. Oxidation of graphite in air is thermodynamically favored at any temperature below 4000 °C. Within the context of this study, only results from very low temperature experiments are relevant: Oxidation reaction have been observed during storage in moist air in the presence of a radiation field and nitric acid. Oxidation of graphite by water vapor is minimal below 1000 °C unless a catalyst is present and, even then, no significant reaction has been reported below 400 °C. Many measurements of graphite oxidation rate in air have been made on small samples of

moderator and sleeve graphite removed from operating reactors in the UK. Similar measurements have taken place in most other gas-cooled reactors. These observations indicate moderate rates of oxidation at 450 °C and an activation energy, which effectively precludes significant oxidation below about 350 °C. These measured oxidation rates reveal a radiation enhancement factor resulting from the activation of reacting surfaces by the neutron flux. Measured oxidation rates in irradiated graphite are found also to be elevated as a consequence of modest amounts of inorganic catalysts. The effect of such catalysts is to increase the graphite-oxidation rate above its normal value at any particular temperature.

Numerous investigations (summarized in [12]) demonstrated clearly that oxidation of graphite is insignificant under disposal conditions at $T \leq 200$ °C, even when air would be present.

2.1.3 Element and Radionuclide Inventory of AVR/THTR fuel elements

Due to their high inventories and relatively long half-lives, ^{14}C and ^{36}Cl are the key radionuclides relevant for the long-term safety of AVR/THTR wastes [13], and additional details are given by Fachinger and Duwe [14]. The ^3H inventory of an AVR/THTR fuel element is mainly generated in the graphite matrix by ^3He and ^6Li impurities. The release is controlled by absorption and desorption processes at the grain boundaries of the graphite and diffusion in the grains. The complete ^3H inventory of a dry storage can amounts to about 2×10^{12} Bq. The ^{14}C inventory is mainly generated by (n-p)-processes of ^{14}N impurities of the graphite. The release of ^{14}C during storage is initiated by corrosion processes of the carbon by contact with air and gamma radiation. In this process, CO_2 will be generated. The inventory of 950 fuel elements amounts up to 7×10^9 Bq. Only 1 % can be released, until the oxygen content of a storage can is consumed. The ^{36}Cl load of the spent AVR/THTR fuels is not reported; for some other radioisotopes inventories are given. The ^{85}Kr inventory is generated by fission and amounts to $\sim 1 \times 10^{13}$ Bq in a storage can. The release mainly depends on the number of defect particles. (Due to the relatively short ^{85}Kr half life of 10.76 a, the ^{85}Kr inventory is relevant to time intervals of the interim storage.) The defect rate of the fuel elements is determined in the range of 3×10^{-4} , which could cause a possible release of 3×10^9 Bq ^{85}Kr per can. Measurements showed a maximum release of 1×10^7 Bq.

A complete list of the radionuclide inventory (in Bq) can be found in [3].

2.1.4 Kinetics of Radionuclide Release from AVR/THTR fuel elements

Investigations of the radionuclide release from spent HTR/AVR fuel elements and from single coated particles have been performed at the Jülich research Center (FZJ) between 1990 and 2000 [14-16]. In the PhD thesis of Zhang [16] four AVR spent fuel elements were investigated. The characteristic data are listed in Tab. 2 and 3.

The leaching behavior was investigated in MgCl_2 saturated solution (Q-brine) at ambient temperature, 55 °C and 90 °C. The leaching progress can be divided into the following processes:

- Diffusion of the solution to the particles within the graphite matrix
- Dissolution of radionuclide bearing phases
- Diffusion of the dissolved radionuclides through the graphite matrix
- Dispersion of the radionuclides in the contacting solution.

Tab. 2 AVR spent fuel elements investigated by Zhang [16]

Experiment No.	AE 85/05 (I)	AE 91/17 [17]	AE 92/14 (III)	AE 92/20 (IV)
Fuel-Type	BISO(Th,U)O ₂ = 10:1	BISO(Th,U)O ₂ = 5:1	BISO(Th,U)O ₂ = 5:1	BISO(Th,U)O ₂ = 5:1
²³⁵ U-Enrichment-	93.0 %	53.0 %	52.3 %	44.3 %
Discharge-	09.07.1988	12.01.1989	12.01.1989	12.01.1989
Burnup (FIMA)	11.50 %	16.89 %	17.11 %	17.11 %

Tab. 3 Measured radionuclide inventory in the AVR spent fuel elements investigated by Zhang [16]

Experiment No.	AE 85/05 (I)	AE 91/17 (II)	AE 92/14 (III)	AE 92/20 (IV)
Mass / gram per fuel element				
Th-232	19.1	4.7	4.68	4.6
U-233	0.38	0.0948	0.0963	0.095
U-234	0.092	n.g.	n.g.	0.023
U-235	0.06	0.1557	0.1456	0.081
U-236	0.288	0.1384	0.1407	0.146
U-238	0.112	0.064	0.064	0.053
U _{tot}	n.g.	0.4691	0.4627	0.303
Pu-238	-	0.0036	0.0036	0.0051
Pu-239	-	0.0014	0.0013	0.0015
Pu-241	-	0.0005	0.0004	0.0006
Pu _{tot}	-	0.0068	0.0066	0.0089
Activity / Bq per fuel element				
Actinides	3.7×10 ¹²	1.84×10 ¹⁰	2.20×10 ¹⁰	n.g.
Cs-134	1.27×10 ¹¹	5.80×10 ¹⁰	6.00×10 ¹⁰	6.11×10 ¹⁰
Cs-137	1.37×10 ¹¹	1.03×10 ¹¹	1.04×10 ¹¹	1.04×10 ¹¹
Eu-154	4.14×10 ⁹	2.60×10 ⁹	2.54×10 ⁹	2.72×10 ⁹
Cs-134	1.27×10 ¹¹	5.80×10 ¹⁰	6.00×10 ¹⁰	6.11×10 ¹⁰

Measurements covered a period of 670 days. In total, the released fraction of ^{134/137}Cs was found in the range of 10⁻⁴ to 10⁻³. ⁹⁰Sr und ¹⁴⁰Ba concentrations were close to the detection limit and no release fraction could be determined. It was shown that the release of radionuclides did not depend solely on the diffusion of the radionuclides through the graphite matrix. The rate-determining process was the release of the radionuclides from the fuel kernels (particles). This rate differed for the fuel matrices UO₂ or (Th,U)O₂. A release from intact TRISO coated particles was not observed. Still, the total inventory of fuel elements contained a fraction of 10⁻⁴ to 10⁻⁵ defect particles. This fraction increased by a factor of about 10 for highly irradiated material. Therefore, the source term for radionuclide release was mainly controlled by the number of defect coated particles [14].

Radiocarbon / ¹⁴C

The ¹⁴C formed in the reactor during irradiation is absorbed at the graphite matrix and incorporated into the crystal structure of the graphite facilitated by the high temperature in the reactor.

Fachinger et al. [13] assumed that within the matrix the preferential location of ^{14}C may be absorbed on the surface of the crystallites rather than integrated into the crystal structure.

The experiments of [14] aimed additionally to determine both the release of tritium and the total ^{14}C inventory, which was converted into $^{14}\text{CO}_2$ and dissolved in the brine. Tritium is not relevant to the source term estimation for long-term disposal of ^{14}C bearing wastes. The authors [14-16] draw the following conclusions on the results of their leaching experiments concerning the coated particles: The data determined clearly demonstrate that the HTR fuel elements were not subject to any measurable corrosion during the 2.5 years leaching period in MgCl_2 rich brine. ^{14}C compounds were detected in some test cycles but found activity values were low. Thus, ^{14}C mobilization from the graphite matrix of the HTR sphere could be ruled out. Moreover, the decreasing activity values of the examined nuclides showed that under these conditions of the experiments, the coatings of the fuel particles remained intact so that only diffusion-controlled leaching of few broken particles took place. The high concentrations of radionuclides and ^{14}C compounds found in the first leaching cycle could be explained by surface contamination and was negligible relative to the radionuclide inventory of the sphere.

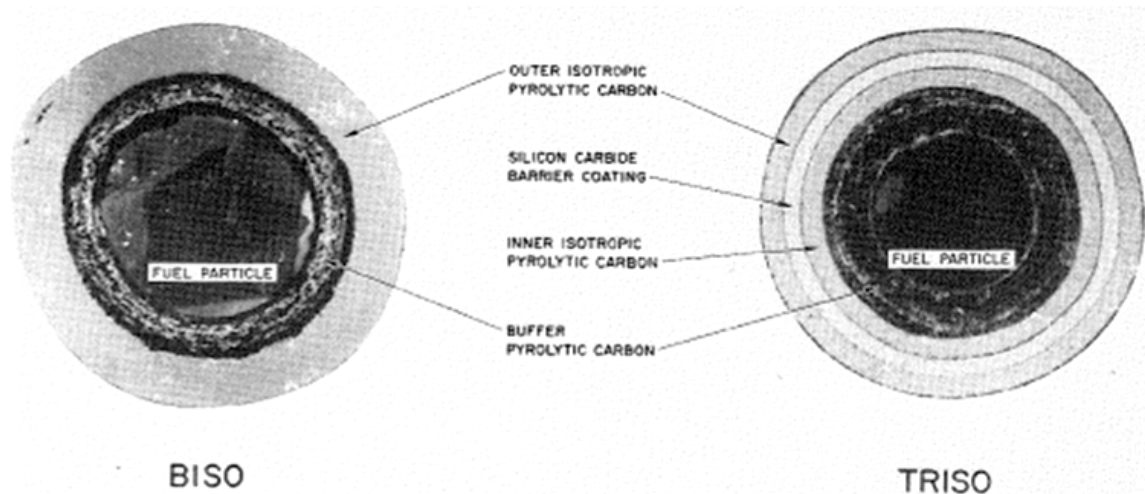


Fig. 2 Cross sections of BISO and TRISO particles [18]

Fachinger and Duwe [14] investigated storage cans AVR-TLK holding 950 AVR fuel elements, each. The long time release of ^{137}Cs was modeled and described as an instantaneous release of about 20% of the inventory, which was related to the amount of defect kernels, and a slow release of the remaining ^{137}Cs in the graphite particles over a time period of several hundred years. Fig. 3 shows the measured ^{137}Cs release for BISO and TRISO kernels over more than 12 years. The long-term release rate for HEU BISO and LEU TRISO can be calculated to a fraction of $2 \times 10^{-9} \text{ day}^{-1}$.

^{14}C was not found in the gas phase but dissolved in the brine. However, the main part of the dissolved ^{14}C occurs not as inorganic compound. The fractional release of organic ^{14}C was determined in the range of 0.014 % after 650 days, the inorganic ^{14}C fraction was below 0.006 %.

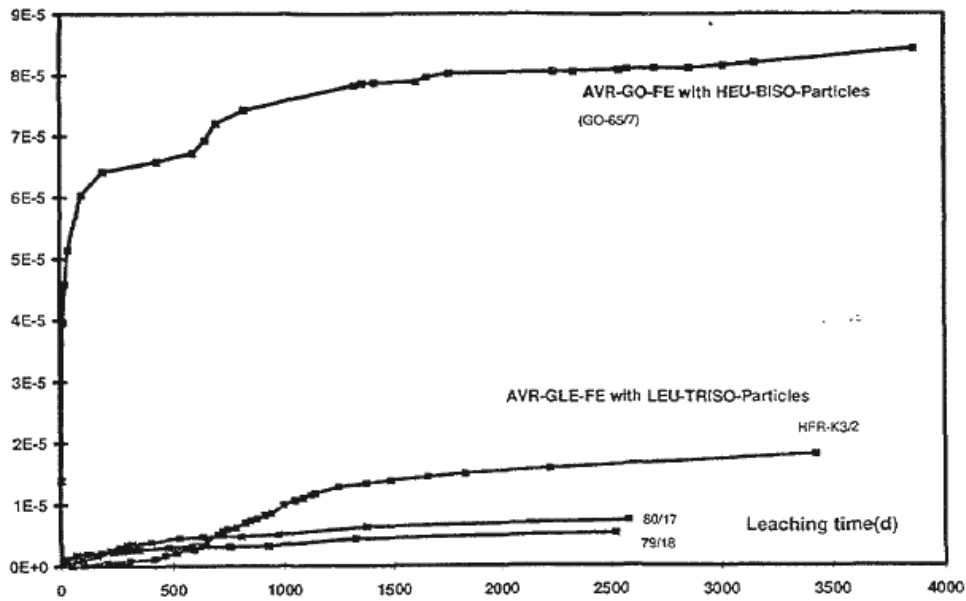


Fig. 3 Fractional release of ^{137}Cs inventory in Q-Brine at 90 °C and 13 MPa [14]

2.2 Fuel elements from the KNK II and the MS Otto Hahn

In total, 2484 fuel rods in 28 fuel elements from KNK II need to be disposed together with 52 fuel rods from NS Otto Hahn, which corresponds to 4 CASTOR KNK casks [3].

2.2.1 Characteristic Properties of KNK II spent fuel

In the period between 1972 and 1991 the sodium-cooled reactor KNK was operated at Research Centre Karlsruhe. Initially KNK I was designed as thermal reactor with a power of 25 MWe. Already during the commissioning of KNK I, it was decided to modify it into a fast nuclear power plant. Until 1977, KNK I was transferred in KNK II. The first fast core was operated from 1977 to 1983 reaching high burnup in the fuel elements. The second core was used from 1983 until the final shut down in August 1991. The history of this sodium cooled reactor is documented by Marth [19].

Each fuel element of KNK I was constructed in a cylindrical shape consisting of a central moderator of ZrH_2 material surrounded by 127 fuel rods. The initial enrichment was 6.75 % ^{235}U . The cladding of KNK I rods was made of austenitic steel with 16 % chromium and 13 % nickel. This steel had a lower tendency of embrittlement by formation of sigma phases compared to steel varieties used abroad with a higher chromium and a lower nickel content. Three types of austenitic steel were tested as cladding material with material numbers 1.4970, 1.4981, and 1.4988.

The fuel elements of KNK II had a length of 2253 mm and consisted of 127 fuel rods each. The fuel rods had a diameter of 7.6 mm and a length of 1556 mm. They were filled with fertile material UO_2 at top and bottom over a length of 2×200 mm and fuel in between over a length of 600 mm [20]. The fuel mass of KNK II was in total 160 kg for the first core and 220 kg for the second core. The fuel was fabricated by ALKEM, Germany, containing high concentrations of plutonium up to 30 wt. %. The density of the fuel was 80 % of the theoretical density. Absorber rods had a slightly bigger diameter (10.3 mm) than the fuel rods and were filled with B_4C . The burnup was up to 100 GWd/t_{HM} . A complete list of the radionuclide inventory of the spent fuel from KNK II can be found in [3]. With respect

to potential reprocessing, dissolution tests were performed at the MILLI plant at Research Centre Karlsruhe for burnups of 11.7 and 74 GWd/t_{HM} [21]. The characteristic data of residues of irradiated fuel elements after dissolution in 7-10 n HNO₃ are given in Tab. 4.

Tab. 4 Characteristics of irradiated fuel samples after dissolution in 7-10 n HNO₃ (Kleykamp [22])

Irradiation experiment / Fuel rod number	KNK II / I 208 BN A1.009	KNK II / I 202 IA A1.1538
Fuel type	U _{0.7} Pu _{0.3} O _{2-x}	U _{0.7} Pu _{0.3} O _{2-x}
Local burnup (FIMA)	1.2 %	4.2 %
Local linear power	29 kW/m	34 kW/m
Residues insoluble in HNO ₃	15 wt. %	14 wt. %
UO ₂ *	50 %	35 %
PuO ₂ + AmO ₂ *	47 % + < 1 %	60 % + 2 %
Fission product alloys*	< 1 %	< 2 %
Fission product oxyhydrates*	0 %	0 %
PuO ₂ **	25 %	30 %

* related to residues, ** related to initial concentration

2.2.2 Characteristic Properties of NS Otto Hahn spent fuel

The nuclear ship “NS Otto Hahn” was one of only four nuclear powered cargo vessels ever built. It had a length of 170 m and was configured to carry bulk goods such as iron ore. The ship was equipped with an advanced pressure water reactor (“fortschrittlicher Druckwasserreaktor” - FDR) using light water for cooling and moderation (overview on technical data given in Tab. 5).

Tab. 5 Characteristic data of the reactor of the NS OTTO HAHN [23]

Thermal power	38 MW
Service time under full load	900 d
Average burnup	23 GWd/t _{HM}
UO ₂ mass per core	1.7 t
Enrichment / average	3.5 or 6.6 % / 4 %
Average thermal neutron flux	$1.1 \times 10^{13} \text{ cm}^{-2}\text{s}^{-1}$
Number of fuel elements / number of fuel rods	12 / 2810
Core diameter	1050 mm
Core height	830 mm
Diameter of a fuel rod	11.4 mm
Wall thickness of the cladding	0.8 mm
Cladding material	Zircaloy-4, partly ZrNb3Sn1
Linear power (1. core / 2. core)	325 / 504 W cm ⁻¹

The reactor was constructed by a consortium of Deutsche Babcock & Wilcox-Dampfkesselwerke AG and INTERATOM, Internationale Atomreaktorbau GmbH and became critical in 1968. A second core was installed in 1972/73 and the ship was decommissioned in 1979. Until 1982, the reactor was

removed and the ship was converted into a diesel fueled container vessel. A complete overview on the characteristics of vessel, reactor, core and operation is provided by GKSS 1981 [24]. The core contained twelve quadratic and four angular fuel elements. Quadratic fuel elements consist of a 17x17 mesh of 289 spaces filled with four structure rods, 32 steering tubes for absorber rods and 253 fuel and burnable poison pins. The uranium enrichment is reported to be either 6.6 % or 3.5 %. The spring in the fuel rods is 59.7 mm \pm 3.5 mm long and made of Inconel X750 and the lower spacer is 62.5 mm long. Burnable poison pins have the same dimensions as the fuel pin. The burnable poison consists of a mixture of ZrO₂ and ZrB₂. The mass ratio of ZrO₂ and ZrB₂ in the mixture was not provided. The only information about the mixture is the mass of boron per unit of length. The control rods consist of B₄C. Further details on the reactor are reported in the context of a MCNP simulation exercise organized by OECD [25].

2.2.3 Element and Radionuclide Inventory of NS Otto Hahn spent fuel

The inventory of elements and radionuclides in KNK II fuel elements from measured and calculated data is given in Tab. 6.

Tab. 6 Comparison between measured and calculated fuel elements in KNK II [26].

	NY-202-IA		NY-203-IA	
	local burnup: 22.8 GWd/t _{HM}		local burnup: 43.8 GWd/t _{HM}	
	Measured	Calculated	Measured	Calculated
U _{total}	29.0 kg	29.9 kg	28.74 kg	29.3 kg
²³⁸ Pu	0.70 %	0.73 %	0.77 %	0.77 %
²³⁹ Pu	77.6 %	77.2 %	78.5 %	78.2 %
²⁴⁰ Pu	14.6 %	14.7 %	14.3 %	15.6 %
²⁴¹ Pu	5.1 %	6.0 %	4.9 %	4.0 %
²⁴² Pu	2.0 %	1.3 %	1.5 %	1.4 %
¹⁴¹ Ce /GBq		0.074	4.81	4.44
¹⁴⁴ Ce/ ¹⁴⁴ Pr /GBq	536.5	610.5	802.9	865.8
¹³⁴ Cs /GBq		5.55	14.8	19.24
¹³⁷ Cs /GBq	103.6	99.9	210.9	188.7
¹⁵⁵ Eu /GBq	7.77	8.51	10.36	14.06
¹²⁵ Sb /GBq		9.99	7.77	16.28
Mo /g		85.2		163.0
Ru /g		56.2		108.0
Rh /g		16.8		31.8
Pd /g		26.2		48.9
Te /g		13.5		25.9

Fuel element NY-202-IA and NY-203-IA were analyzed for the core and the breeding zone separately. NY-202-IA consisted of 13833.0 g ²³⁵U, 1041.0 g ²³⁸U, and 6388.0 g Pu in the core zone and 39.0 g ²³⁵U, 15614 g ²³⁸U and no Pu in the blanket. NY-203-IA had 13512.1 g ²³⁵U, 1177.1 g ²³⁸U, and 6114.4 g Pu in the core zone and 31.7 g ²³⁵U, 15793.0 g ²³⁸U and no Pu in the blanket. NY202-IA was irradiated for 192.5 days at an average burnup in the core of 39.1 and 0.63 GWd/t_{HM} in the blanket. Burnup of

NY-203-IA was 76.0 GWd/t_{HM} in the core zone and 1.2 GWd/t_{HM} in the blanket; the irradiation period was 400 days.

2.2.4 Kinetics of Radionuclide Release of NS Otto Hahn spent fuel

Due to the fact that the ship was navigated in ports and densely used sea routes, the power load needed to be changed frequently in the range between 18 % and 95 % of the continuous power. The power load changes had a rate of 1 % s⁻¹. Up to 60 load changes took place within 8 hours.

The kinetics of the radionuclide release from the fuel elements of the NS Otto Hahn is controlled less by the relatively slow burn-up of the UO₂ fuel, but more by the frequent changes in the power load and the related temperature changes. It is assumed that the UO₂ matrix is heavily disturbed and fractured. Therefore, the fraction of instantly released radionuclides is estimated to be in the upper range compared to spent fuel from power reactors.

2.3 Fuel elements from the research reactors BER II and FRM II

Research reactors are used for the production of neutrons for material investigations, for neutron activation analysis, and for testing newly developed fuels. The irradiated fuel assemblies with highly-enriched uranium are considered as waste.

Ten training and research reactors were in operation in Germany in 2009 [27]. These are:

- two materials test reactors (MTRs) (Berlin and Geesthacht)
- one high-flux reactor (Munich),
- one TRIGA reactor (Mainz)
- six training / educational reactors, including five Siemens educational reactors (SUR).

Presently, three research reactors, the FRM-II (München), the FRG-I (Geesthacht) and the BER-II (Berlin) with a thermal output higher than 5 MW are in operation in Germany. The Jülich research reactor (FRJ-2) was finally shut down on 2 May 2006 and is currently in the post-operational phase. Five Siemens educational reactors (SUR) and one training reactor still have a valid license for operation. Three of these (Stuttgart, Ulm, Furtwangen) are supposed to continue their operation. The other two SURs (Aachen, Hanover) will be decommissioned. A precondition for their decommissioning is the removal and disposal of their reactor cores. In the reactors FRMII and BERII, dispersed U₃Si₂-Al-fuel is used. Older research reactor types made use of dispersed metallic UAl_x-fuel. It was planned to return the irradiated research reactor fuel elements of US origin if these fuels were discharged from the reactor not later than May 2006.

The U₃Si₂-Al-fuel is stored and has to be disposed of. In 2007, there was approx. 0.8 Mg of spent fuel assemblies from these reactors waiting for disposal. The fuel assemblies from the MTR facilities Berlin, Geesthacht and Jülich are foreseen for return and disposal in the US. However, according to the current legal situation, this disposal path is only an option for fuels that have been irradiated until May 2016. Should the reactor core continue operation beyond that date and should there be no prolongation of the contract for shipping the waste to the US, then the fuel assemblies will be sent to the central interim storage at Ahaus. This also applies to the TRIGA reactor in Mainz, which according to current plans will stay in operation at least until 2020. As for the FRM II research reactor, the

current legal situation impedes the return to the US. The TRIGA fuel assemblies will therefore also be stored in the interim storage at Ahaus.

In total, this waste amounts to 120 fuel rods from BER II packed into 20 CASTOR MTR casks, as well as 120-150 fuel rods from FRM II corresponding to 30 CASTOR MTR casks [3, 4].

2.3.1 Characteristic Properties of FRM II

The following characterization is based on information from the web page of the Technical University of Munich (TUM) [28]: The concept of FRM II is based on the use of a compact core containing a single cylindrical fuel element installed in the centre of a moderator tank filled with heavy water. Cooling is performed with light water from the reactor pool. The reactor is controlled by means of the central control rod inside the fuel element. To shut it down, an additional, independent system of five shutdown rods is provided in the moderator tank. Each system is individually capable of shutting the reactor down quickly and permanently at any time. The compact construction of the fuel element means that more than 70 % of the neutrons leave the uranium zone and build up to a maximum thermal neutron flux density (undisturbed $8 \times 10^{14} \text{ cm}^{-2} \text{ s}^{-1}$) at a distance of 12 cm from the surface of the fuel element.

The fuel U_3Si_2 composed of a mixture of uranium silicates and aluminum powder is pressed, then it gets boxed in a frame of aluminum and sealed by a cladding of aluminum. These components get cold welded into the fuel plate. The length of the plate increases ten times and the thickness decreases at a value of 1.36 mm. These specially treated fuel plates ensure that the radioactive fission products stay locked in. The 113 fuel plates are each 1.36 mm thick and have an involute shape (see Fig. 4). Therefore the cooling gaps exhibit a constant width (2.2 mm). In order to homogenize power and fission density, the uranium content in the outer zone of each fuel plate is reduced from 3 g cm^{-3} to 1.5 g cm^{-3} . Furthermore a boron ring is employed at the lower end of the fuel element to level the power density in this region.



Fig. 4 Fuel element consisting of 113 involute fuel plates (according to TUM FRM II Homepage [28]). The control rod, which moves inside the fuel element, is not shown.

The moderator tank is equipped with five hafnium absorber rods. Four of them are sufficient to keep the reactor subcritical. The central control rod is positioned in the inner canal of the fuel element. During normal operation the central control rod is pulled up to compensate the burn-up of the fuel

element. This rod is divided into an absorbing front section and a reflecting end section, in order to achieve a higher burn-up of the fuel.

Diameters of the fuel element and the central absorber rod are 243 mm and 118 mm with a height of approx. 700 mm. Including its packaging, the fuel element is approx. 1.3 m high. With a cycle length of about 50 days, 5 fuel elements will be required per year.

2.3.2 Characteristic Properties of BER 2 fuel

The BER 2 core contains of 30 to 40 fuel elements. Each is constructed of 23 thin plates consisting of an aluminum mantle which confines a uranium silicate compound. Characteristic data of the reactor concept have been reported by Axmann and Didier [29] (see Tab. 7). Further details are available on the web page of Helmholtz Zentrum Berlin [30]. It is planned that the spent fuel will be transferred to the USA until May 2016 [27].

Tab. 7 Characteristic data of the BER-2 reactor according to Axmann and Didier [29]

Start of operation	1991 / 2000
Maximum thermal flux	$2.0 \times 10^{14} \text{ n cm}^{-2} \text{ s}^{-1}$
Power	10 MW
Enrichment	HEU 93 wt. % ^{235}U until 1997, LEU since 2000
Type of fuel elements	MTR
Number of fuel elements (FE)	24 FE with 322 g ^{235}U each, 6 "control elements" carrying control rods with 238 g ^{235}U
Size of the core	1 m^3
Mass of uranium	180 g per fuel elements (total: 5.4 to 7.2 kg)
Power density	$2200 \text{ kW (kg U)}^{-1}$
Power density	110 kW dm^{-3}
Reflector	Beryllium
Cooling	Light water
Control	One of six absorber pins
Shut down	Six absorber pins

2.3.3 Element and Radionuclide Inventory

A complete list of the radionuclide inventory (Bq) in BER II and FRM II fuel elements is given in [3].

2.3.4 Kinetics of Radionuclide Release

Investigations of MTR fuels have been performed since 1990 to a large extent by Helmholtz Zentrum Jülich. Summaries of the results were published in several reports and an edited book by Rammelmaier et al. [31-33]. The investigations on radionuclide release from $\text{U}_3\text{Si}_2\text{-Al}$ -fuel included the following steps:

- Corrosion of pure aluminum
- Leaching of spent MTR fuel pieces
- Remobilization from secondary phases

The findings are given in [31]:

- The Al-matrix of the spent fuel element will be disintegrated instantaneously in salt brines with respect to the relevant time periods of a final repository. The corrosion rate in saturated NaCl was ~ 10 wt. % year⁻¹, in MgCl₂-rich solutions, complete corrosion took place within < 20 days.
- The presence of iron corrosion products from storage casks speeded up the corrosion reaction.
- Corrosion products of the aluminum precipitate formed a secondary Al-phase Al-Cl₃ · 4Al(OH)₃ · 7H₂O and Mg₂(OH)₃Cl · 4H₂O.
- The precipitates immobilized radionuclides especially actinides.
- In brines with a high chloride concentration, primarily sorbed α -emitters were firmly bound to the secondary phases.

Some studies on sorption of FP onto the Al precipitates have been performed, mainly in the pH range $0 \leq \text{pH} \leq 6$. Experiments currently performed within the BMWi funded VESPA project study the retention of radionuclides in Al compounds, such as hydrotalcite. Since the project is still ongoing, final data are not yet available.

2.4 Graphite Wastes

Graphite is a form of carbon that occurs naturally in the environment and can also be manufactured. For the UK Magnox reactors, graphite is manufactured in the form of bricks, which surround the fuel and are used to moderate or slow down the nuclear reaction. The details on graphite behavior that are described in the following are mainly taken from IAEA TECDOC 1521 “Characterization, Treatment and Conditioning of Radioactive Graphite from Decommissioning of Nuclear Reactors” [12].

Approximately 1000 m³ of “graphite” wastes are waiting for disposal in Germany. Other countries such as UK and France have operated Magnox and Advanced Gas-cooled Reactors (AGRs) where a considerably higher amount of irradiated graphite was produced. With more than 99000 tons (79000 m³), the UK has the largest graphite waste inventory in the world. Categorized as Intermediate Level Waste, the waste originates from operational and reactor decommissioning activities [34].

Compared to other forms of ILW, graphite waste is chemically stable and presents a relatively low hazard, though containing long-lived radionuclides. In the UK, it is currently destined for burial in a geological disposal facility where it will account for 33 % of the available space.

2.4.1 Characteristic Properties of Graphite Wastes

Characteristic properties of graphite waste are similar to those of BISO and TRISO graphite waste. As described in section 2.1.1, oxidation of graphite is not relevant under disposal conditions.

Graphite dust must be distinguished from other impure carbonaceous dusts (like coal dust) which are easily explosive. Nuclear graphite dusts are found to be much less reactive due to the lack of volatiles and the particle size, which is primarily responsible for the different behavior of graphite dust and other impure carbonaceous dusts. The question of explosiveness of impure graphite dust containing stored energy was discussed in UK in the context of its relevance for graphite-handling operations during reactor decommissioning and subsequent graphite storage or disposal.

Under disposal conditions, however, graphite dust explosions are not relevant.

Graphite may react electrochemically with other materials. Acting as a “noble” metal, it can promote accelerated corrosion of other metals by electrical (galvanic) coupling, in which local electrolytic cells driven by potential differences lead to increased dissolution and oxidation of less noble metals. Graphite is more electronegative even than stainless steel, so that direct contact between graphite wastes and stainless steel containers can lead to premature penetration and loss of integrity. Experimental studies have shown that corrosion rates can be increased by factors of up to ten [12].

A number of measures for prevention have been identified, including use of cement grouts and baskets to isolate graphite from stainless steel waste containers.

Tab. 8 Characteristic data of the graphite wastes [3]

approximate waste volume (net / gross volume)		m ³	1000 / 2990
mean density		g cm ⁻³	2.2
container type for storage		MOSAIK or Konrad type IV	
container	steel/iron	Mg	13519
	resin	Mg	5
waste inventory	carbon bricks (“Kohlestein”)	Mg	1540
	graphite	Mg	660
	residual moisture	Mg	10

2.4.2 Element and Radionuclide Inventory in graphite wastes

Tab 9 lists the radionuclide inventory of the graphite-containing wastes [3].

Tab. 9 Radionuclide inventory in the graphite-containing wastes [3]

	Activity / Bq per fuel element
H-3	2.5×10^{15}
C-14	2.8×10^{14}
Cl-36	5.8×10^{10}
Co-60	7.1×10^{13}
Sr-90/Y-90	1.6×10^{13}
Cs-137	3.2×10^{12}
Eu-154	1.1×10^{11}

2.4.3 Kinetics of Radionuclide Release from graphite wastes

The leaching of ¹⁴C and ³⁶Cl from irradiated French and Hanford reactor graphite were investigated [35, 36]. The leach rates were measured on solid cylindrical samples of graphite prepared from a bar retrieved from spacer bars that had been irradiated in one of the obsolete Hanford production reactors. Static leach tests were conducted in deionized water and Hanford ground water at temperatures of 20 - 90 °C for 8 weeks. The graphite samples were completely submerged in the leachant, and the entire volume of leachant was changed and analyzed weekly. The leach rates of both ¹⁴C and ³⁶Cl decreased with time and appeared to approach steady-state values that were independent of temperature in the case of ³⁶Cl but decreased with temperature in the case of ¹⁴C.

Corrosion of nuclear graphite in MgCl_2 - and NaCl -rich solutions and pure water has been studied by [37]. It was shown under oxidizing conditions that corrosion rates in the high ionic strength solutions were lower than in water. Rates were controlled by oxidation of carbon to CO_2 upon reaction with dissolved oxygen. In γ -irradiation experiments, however, rates were higher in the chloride-rich solutions than in pure water due to the presence of radiolytically produced oxidants.

Under reducing conditions, as will be expected in the repository, we can therefore assume low corrosion rates. For both isotopes, an average mass loss rate under oxidizing conditions was determined in the range of 4.7×10^{-10} to $1.9 \times 10^{-11} \text{ g m}^{-2} \text{ day}^{-1}$ in water at 20°C .

2.5 Compacted structural materials from conditioning of spent LWR fuel elements

Compacted structural materials from conditioning of spent fuel elements from LWRs may be produced in the Pilot Conditioning Plant (PKA) at Gorleben. Since 1980, the construction of the PKA has taken place at the Brennelementlager Gorleben site. The PKA was designed as a multi-purpose facility to fulfil various tasks within the framework of conditioning and managing spent-fuel assemblies and radioactive waste. The pilot character of the plant allows for the development and testing in the field of spent-fuel-assembly conditioning. The objectives of the PKA may be summarized as follows: Conditioning of spent-fuel assemblies, reloading spent-fuel assemblies and waste packages, conditioning of radioactive waste, and conducting maintenance work on transport and storage casks as well as on waste packages [38]. Further papers describing the PKA and the waste conditioning techniques have been published [39, 40]. A schematic illustration of the structural parts of a fuel assembly is shown in Fig. 5. The first step for disassembling a fuel assembly is separating of the head and bottom parts. At most of the BWR/PWR assemblies this is done by unscrewing. At some fuel assemblies the control rod guiding tubes have to be separated by a special cutting device.

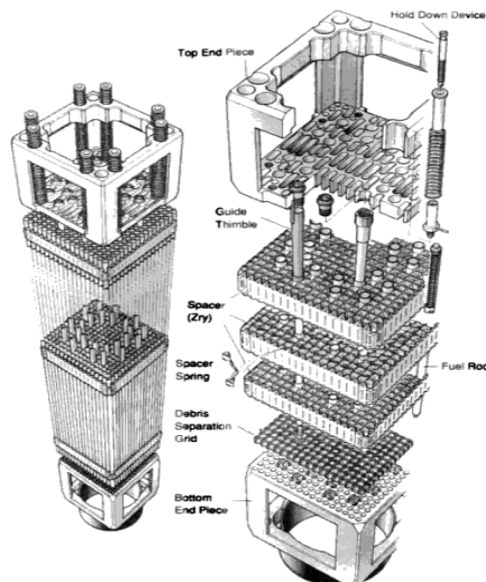


Fig. 5 Schematic illustration showing the structural parts of a BWR Siemens ATRIUM 9x9 fuel assembly [41]

For compaction of structural parts of fuel assemblies, a 5000 kN skeleton press has been developed. This press will compact the fuel element skeletons composed of head and bottom parts as well as

spacers with water guiding tubes. During the testing PWR and BWR skeletons as well as also Zircaloy fuel channels of BWR were compacted. The result was highly compacted metal block with a volume reduction of 1:8.

Due to the required long distance of compacting of 5 meters the press ram is composed of five parts which are placed one after the other into the press box. This technique makes it possible to provide a relatively short length of the press, with a disadvantage that the time of compacting for a skeleton amounts to approx. five hours [39].

2.5.1 Characteristic Properties of compacted structural material

Composition and properties of the compacted metals are similar to those of the CSD-C wastes, however fuel rod cladding material is not expected to be present. For this reason, it is referred to the previous report on "Radionuclide source term for HLW glass, spent nuclear fuel, and compacted hulls and end pieces (CSD-C waste)" [1]. The structural materials of the fuel assemblies consist of 4.44 kg Inconel per PWR fuel element with 7 – 18 wt. % Fe and < 2000 ppm Co. Additionally, Zircaloy is a component of the fuel assemblies: it originates from spacers, grids, and control rod guiding tubes (up to 24 per PWR fuel element) as well as sheets for controlling the coolant flow in the reactors. The amount of Zircaloy in the structural materials of one PWR fuel element (without hull) is 32.88 kg [3].

2.5.2 Element and Radionuclide Inventory of compacted structural material

The volume of compacted structural materials amounts to 630 m³. The inventory of the compacted hulls and end pieces is given in Tab. 10, while the radionuclide inventory is given in [3].

Tab. 10 Inventory of the compacted structural materials including waste package [3].

		Mass [Mg]
Container material	Steel/iron	15388
	Lead	9421
	Resins	5.5
Inventory of waste	C	0.8
	Si	8.2
	Cr	162.2
	Mo	0.9
	Ni	146.5
	Al	2.2
	Nb	2.3
	Ti	5.6
	Fe	568.6
	Mn	15.3
	P	0.4
	S	0.2
	Co	1.8
Moisture	Residual water	5

2.5.3 Kinetics of Radionuclide Release

Corrosion behavior of zircaloy-4 was investigated in saturated NaCl solution, MgCl₂-rich brine and bentonite water [42]. Corrosion rates of < 0.1 μm/yr. were measured. In the presence of H₂ gas formed by corrosion of steel, Zircaloy-4 shows a strong tendency of embrittlement [43]. ZrH₂ is formed rapidly onto the grain boundaries and influences the mechanical properties of the zircaloy negatively. In spite of the low corrosion rate of zircaloy, it can be expected that shortly after the formation of a H₂ gas pressure, the zircaloy hulls degrade. The radionuclide release of cladding material was investigated in saturated NaCl solution for 83 days at 200 °C. Corrosion was initiated only after 100 ppm fluoride was added to the leaching medium. The observed mass loss after 83 days was 0.087 g (2.4 %) for the PWR and 0.059 g (1 - 2 %) for the BWR materials. The ¹⁴C results obtained under these conditions indicated that cladding corrosion mobilizes about 50 % of the ¹⁴C in PWR hulls and about 90 % of the ¹⁴C in BWR hulls. The mobilized ¹⁴C was found ~95 % in the ¹⁴CO/¹⁴CH₄ fraction, whereas ¹⁴CO₂ at ~5 % represented a minor part.

A "Progress Report on Disposal Concept for TRU Waste in Japan, 2000" quoted in [44] defined the radionuclide release from cladding material in the Japanese reference case as instant release of the oxide film on the zircaloy and complete dissolution of the metal within 7600 yrs. For BWR cladding after 39.4 GWd/t_{HM}, the oxide film was 2.2 wt. % of the zircaloy metal. According to [45] who cite a former study of Yamaguchi et al. [46], 17 % of the ¹⁴C in cladding is present in the oxide film so that the concentration of ¹⁴C in the oxide film is at least 3 - 4 times that in the underlying alloy.

2.6 Tails from uranium enrichment

A large amount of depleted uranium is generated during enrichment of uranium. Disposal of this waste is considered within disposal concept A.

2.6.1 Characteristic Properties of tails from uranium enrichment

The term "tails" refers to depleted UF₆ with 0.2 - 0.3 % ²³⁵U [47]. For disposal, it is planned to transform the uranium tails from the enrichment process into U₃O₈, which is also produced from UF₆ during nuclear fuel production. After conversion to U₃O₈ the tails may additionally contain resins, up to 2 % uranylfluoride UO₂F₂ as well as unreacted hydrofluoric acid (HF) at an unknown concentration.

The U₃O₈ compound can be produced by any one of three primary chemical conversion processes, involving either UF₄ or UO₂F₂ as intermediates. It is generally considered to be the favored form for disposal purposes because, under oxidizing environmental conditions, U₃O₈ is one of the most thermodynamically stable forms of uranium. Its particle density is 8.3 g cm⁻³. Uranyl fluoride (UO₂F₂) is an intermediate in the conversion of uranium hexafluoride UF₆ to uranium oxide and is formed by the reaction of UF₆ with moisture in the air. It is very soluble in water. Uranyl fluoride is stable in air to 300 °C, above this temperature, it slowly decomposes to U₃O₈. When heated to decomposition, UO₂F₂ emits toxic fluoride fumes.

According to geochemical calculations, no solid effectively constrains the UO₂²⁺ concentrations for pH < 7 under oxidizing conditions. At higher pH, the Ca/Na uranate phases control the U concentrations at values below 10⁻⁶ mol/L.

2.6.2 Element and Radionuclide Inventory

In [3], the activity of the tails is reported in terms of Bq per Mg U_3O_8 : 1.80×10^9 Bq/Mg ^{234}U , 1.43×10^8 Bq/Mg ^{235}U , 1.07×10^{10} Bq/Mg ^{238}U . The ratio of $^{235}U/^{238}U$ reveals a depletion ratio of 0.2 %.

The reported waste volume adds up to 35000 m³ of uranium tails, which will be stored in 7217 “Konrad” containers of type VI resulting in 15 520 kg tails per waste package. Detailed information on the inventory is given in Tab. 11.

Presently, there is no knowledge on contamination with fission products from reprocessed uranium.

Tab. 11 Inventory of uranium tails including waste package [3].

		Mass [Mg]
Container material	Steel/iron	9743
	Resins	59
Inventory of waste	U_3O_8	109760
	UO_2F_2	2240
	Residual moisture	550
		Mass [%]
Isotopes	^{234}U	9×10^{-4}
	^{235}U	0.2
	^{238}U	99.799

2.6.3 Kinetics of Radionuclide Release

The uranyl fluoride (UO_2F_2) is supposed to be distributed homogeneously in the U_3O_8 tails and to dissolve immediately when water or brine contacts the material. Therefore one has to assume an instant release of the uranyl fluoride. No information is available on the particle size of the U_3O_8 tails.

2.7 Other mixed wastes with negligible heat generation

2.7.1 Characteristic properties of the mixed wastes

15000 m³ of additional wastes need to be considered, which might not fulfill the requirements of a repository for low- and intermediate level wastes. A model inventory has been assumed [3], since the exact composition of these wastes is not known.

2.7.2 Element and Radionuclide inventory

The estimated total inventory is given in Tab. 12, while the nuclide-specific activity inventory can be found in [3].

EDTA is a polyamino carboxylic acid, which acts as a hexadentate ligand and chelating agent. After being bound by EDTA, metal ions remain dissolved and exhibit a lowered reactivity. For this reason, EDTA is used in many industrial applications. EDTA complexes show a significantly higher thermodynamic stability compared to weaker ligands such as citrate, oxalate, or iso-saccharinic acid.

Tab. 12 Total inventory of the mixed wastes with negligible heat generation [3].

		Mass [Mg]
Container material	steel/iron	11651
	concrete/cement	23881
	lead	1728
	resins	24
	plastic	12
Immobilization material	concrete/cement	8009
	bitumen	136
	plastic	49
Inventory of waste	cellulose	27.4
	EDTA [*]	2.8×10^{-4}
	complexing agents ^{**}	2.5×10^{-1}
	surfactants ^{***}	1.42×10^{-1}
	other organic components	12.2
	inorganic carbon compounds	453
	Al	458
	Zr	77
	concrete/cement	1494
	plastic/petroleum	374
	steel	1256
	other inorganic compounds	2024
	ashes	79
	Zn	0.2
	Be	1
Moisture	bound water	4849
	pore water	861
	other ^{****}	44
	structural water	84
	unbound water	24

* Fe(NH₄)-EDTA, Na₂-EDTA; ** other than EDTA: Na₃-citrate, K₃-citrate, Na₂-hydrogen citrate, (NH₄)₂-hydrogen-citrate, Na₂-tartrate, Na₂-oxalate; *** anionic, nonionic and cationic surfactants; **** water that could not be classified any further

2.7.3 Kinetics of radionuclide release from other mixed wastes

The kinetics of radionuclide release from the other mixed wastes is discussed in Sections 2.8 and 2.9 together with the release from cemented and bituminized wastes.

2.8 Cemented waste forms

Cementation of liquids is considered as an appropriate option for treatment of low-level and intermediate-level waste (LLW and ILW, resp.). Conferences organized by IAEA in 1960 (Vienna), 1965

(Vienna) or 1970 (Aix-en Provence) demonstrated the widespread use of cementation for solidification of radioactive wastes in many countries at this time – and cementation of low-level radioactive wastes is still in use on an industrial level. Portland cement is widely used for solidification of radioactive wastes. The exact composition of the cement is subject to regional variations, since cement is produced from natural resources, such as limestone (calcium carbonate) with small quantities of other materials (e.g. clays). During calcination (1450 °C), the cement clinker is blended with the other materials that have been included in the mix. Frequently, cement kilns are used for incineration of industrial waste. The hydration of the clinker is controlled by addition a certain amount of gypsum after the calcination process.

Special cement mixtures have been developed for the requirements of waste conditioning. The “Portland-Zementwerke Heidelberg” developed the mixture “Addiment Trockenbeton KW 1 to KW 4”. Especially the dry concrete mixtures KW 3 and KW 4, which contain 10 wt. % of sand, have been used for the solidification of evaporator concentrates from nuclear power plants. The sand improves the miscibility of the cement powder with the waste solutions and reduces the tendency for cracking. The KW 3 contains a high proportion of borate binding additives, and is accordingly used for waste of high boron content (upper limit at 45 000 ppm borates in the concentrate). Borates slow down the setting of cement whereas in the presence of lime, solid calcium borate phases precipitate. Another cement mixture for the spilling solid wastes is “Maxit 2000” developed by Kalkwerk Mathis. The mortar has a sufficiently low viscosity to fill all voids in the waste drums and provide for a sufficient compressive strength. The exact compositions of these special cement compositions are protected by trade secret.

Concrete additives are used to impact the viscosity of the cement paste, to reduce the setting time, and to stabilize the unhydrated mixtures in order to avoid bleeding and sedimentation. These additives are used in quantities of $< 50 \text{ g kg}^{-1}$ cement powder. According to Glaus 2004 [48], the admixtures may react with radionuclides in solution (complexation) and compete for surface sites with radionuclides or other strong complexants sorbing on cement phases. Concrete admixtures used at the Paul Scherrer Institut (PSI), such as sulfonated naphthalene-formaldehyde condensates, lignosulfonates and a plasticizer for waste conditioning, were subjected to screening experimental investigations at PSI. For the results of the experiments, it is referred to Section 3.4 on complexing agents.

2.8.1 Characteristic properties of cemented waste forms

Corrosion of cement or cemented waste forms are subject to several processes: (1) The pores of the cement are connected to the surrounding aqueous phase and diffusion processes take place. These effects the dissolved and easily soluble components of the system, e.g. Cl^- , Na^+ , Ca^{2+} , Mg^{2+} , nitrate. (2) In the case of Mg containing solutions, Mg-hydroxides or Mg-oxychlorides (depending on the MgCl_2 -concentration) precipitate at pH-values exceeding ~ 8.7 . This reaction causes the Ca – Mg exchange, where Ca^{2+} compensates the charge balance. (3) Due to the dissolution of portlandite and the Ca – Mg exchange or increase of pH outside (pH plume), the pH of the cement decreases and the calcium silicate hydrates and other cement phases become thermodynamically instable and degrade. (4) Reactions with components of the solutions, such as sulfate or carbonate in the pores of the cement products form solids of a different specific volume generating tensile stresses within the cement. These stresses lead to a mechanical degradation. These processes have been described in numerous publications and textbooks (e.g. [49, 50]).

A summary of the physical and chemical properties of cemented waste forms is given by Vejmelka et al. [51]. The leach and corrosion rate was considered to be one of the most significant criterions for

assessing the quality of cemented radioactive wastes. In order to evaluate the applicability of results obtained by investigations of laboratory samples to real size waste forms and to evaluate the effects of the technical production process, corrosion and leach test have been performed also with full-size cemented waste simulates in the 1970s in German research facilities (Forschungszentrum Karlsruhe and Asse II salt mine) [51, 52]. Initially, the objectives of these experiments covered mainly the technical cementation process, the water to cement ratio (W/C) and the pore structure of the product, the waste load and additives, as well as size and geometry of the samples. During the duration of these experiments, the objectives of the tests were extended and cover now the long-term release of matrix components, formation of secondary phases and the release of radionuclides in terms of kinetics and thermodynamics.

A variety of analytical methods was applied to retrieve information on composition and mineral phases in the cemented waste forms before and after their exposure to NaCl and MgCl₂-rich solutions for periods up to 30 years. A summary is provided by Kienzler et al. 2008 [53]. XRF, XRD, DTA gave average values, whereas scanning electron microscopy SEM-EDX resulted in details of single phases in a scale of some μm. All methods have specific detection sensitivities, and the combination of the different methods support the highest feasible degree of information. The following statements could be proven:

- Mechanical properties: For disposal, the compressive strength of cemented waste forms is of relevance. It was not possible to measure the compressive strength directly; therefore elastic modulus, shear modulus and Poisson's ratio were determined showing significant deviations from uncorroded cement products for the NaCl system. In consequence, the compressive strength of corroded cemented waste forms is by orders of magnitude below values obtained for pristine product.
- Distribution of radioactive and non-radioactive waste components showed partly heterogeneous distribution patterns for both ¹³⁷Cs, U_{nat} and for NO₃⁻. It was suspected that these patterns resulted from artifacts during preparation of the simulated waste forms.
- Thermogravimetric investigations showed the free water content of the samples in the range of 13 - 20 wt. % for the MgCl₂ systems and 12-14 wt. % for NaCl systems. Solid carbonates were found in negligible amounts in the corroded waste forms after more than 20 years. Carbonates contributed to the mass loss only by 1.5 – 2.8 wt. % even in the case of the high pH conditions of the NaCl systems.
- Element analyses showed only slight radial dependence with respect to chloride indicating complete corrosion of the samples during the time of exposure.
- By XRD and SEM mineral phases are identified, such as halite, brucite, calcite, ettringite, gypsum, Mg-oxychloride and (Mg,Ca)-Al-chlorohydroxides (Friedel's salt).

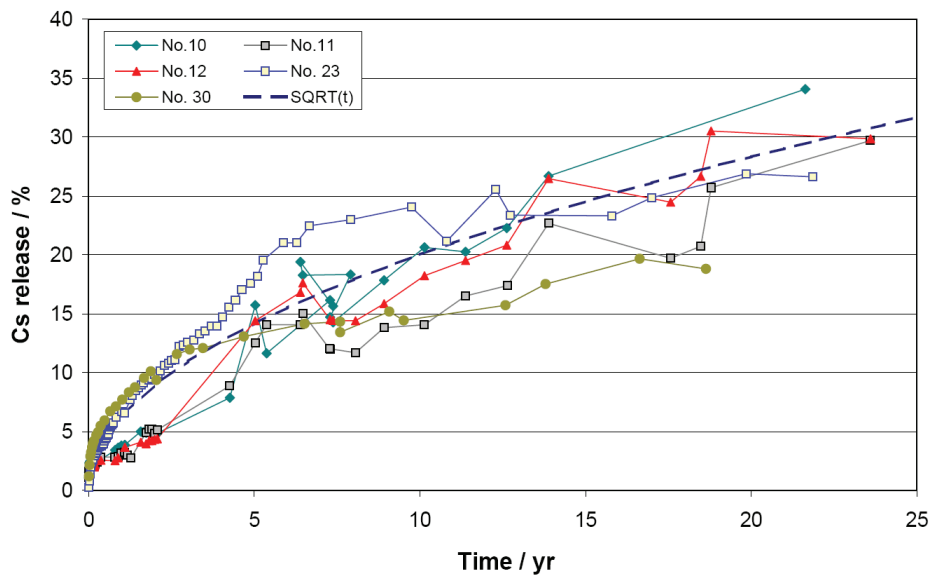
In summary, the various analytical methods complement one another. Results obtained by averaging methods like XRF, XRD, DTA and the results of microscopic detail analyses of single phases or phase agglomerations agree well. The results indicate that the corrosion processes of the cement products in NaCl and MgCl₂ solutions (W/C 0.4 - 0.5) had reached equilibrium with the solutions.

2.8.2 Element and Radionuclide Inventory

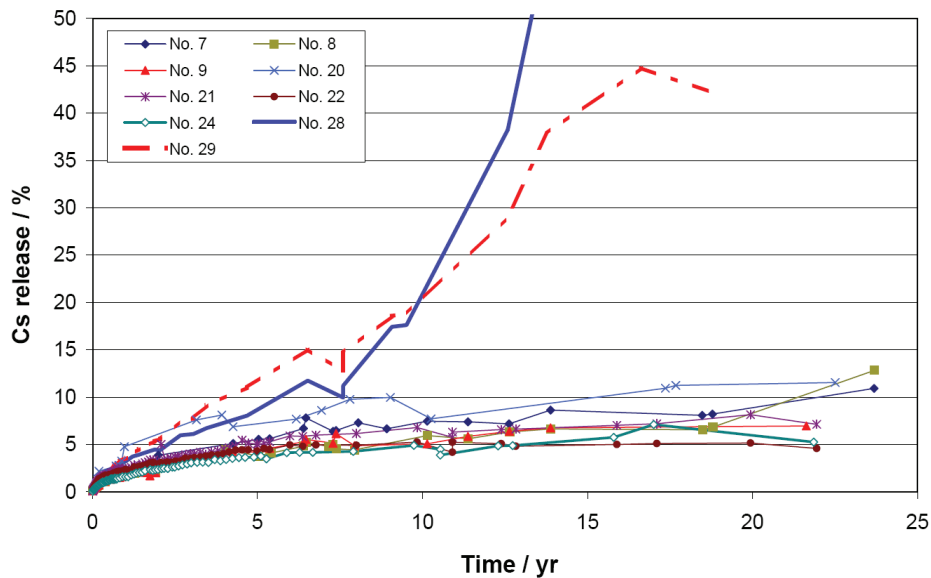
It is referred to the list of the radionuclide inventory (Bq) in [3].

2.8.3 Kinetics of Radionuclide Release

The kinetics of radionuclide release from cemented waste forms depends strongly on the water to cement ratio of the waste form and the brine composition. The measured Cs release from simulated full-scale cemented waste forms is shown in Fig. 6. The waste forms submerged in NaCl solution showed a diffusion controlled radionuclide release. After 25 years, between 20 and 30 % of the Cs inventory was found in the solution. For samples stored in MgCl₂-rich solutions (“Q-brine”), the findings are different. Samples with low W/C ratios showed also a diffusion controlled Cs release over ~25 years. The total release was between 5 and 15 % of the inventory. Samples with realistic W/C ratio of 0.5, however, degraded mechanically in a relatively short time and almost the complete Cs inventory was found in the attacking brine. This behavior was found also in full-scale test performed at INE [54]. The diffusively controlled release of easily soluble substances from the waste forms is corroborated by investigations of nitrate which was a main component of such waste forms [55].



a) NaCl systems



b) MgCl₂ systems

Fig. 6 Observed Cs release from simulated full-scale cemented waste forms [56].

Diffusion coefficients for some substances released from cemented waste forms in saturated NaCl solution have been determined for full-scale samples [55] and are listed in Tab. 13.

Tab. 13 Fitted apparent D_a and diffusion coefficients of water D_w , D_{exp} obtained from small-scale laboratory tests and retention ratio D_a/D_w . Data taken from [55], if not indicated.

	$D_a /$ $m^2 s^{-1}$	D_w [57] $m^2 s^{-1}$	$D_{exp} /$ $m^2 s^{-1}$	D_w/D_a
Cl^- (sample #31)	2.3×10^{-11}	2.0×10^{-9}		88
NO_3^- (sample #30)	1.0×10^{-11}	1.9×10^{-9}		410
NO_3^- (sample #31)	4.6×10^{-12}	1.9×10^{-9}		83
Cs^+ (sample #30)	5.8×10^{-13}	2.1×10^{-9}	2.7×10^{-13} [51]	3552

A K_d of Cs^+ onto cement phases in NaCl solutions was found in the range of 0.5 ml g^{-1} . This Cs^+ retention value for cement corroded in saturated NaCl solution is within the expected range [58].

The release of uranium showed a different behavior and indicates that U-concentration is controlled by the solubility of a U(VI) solid phase. Fig. 7 shows a fast increase of the measured concentration. After more than 20 years, the concentrations did not exceed the concentrations which were measured shortly after the start of the experiments. The evolution of the U-concentration and pH strongly depends on the composition of the leaching solution and the initial W/C ratio. For details on the experiments, it is referred to previous publications [54, 59, 60].

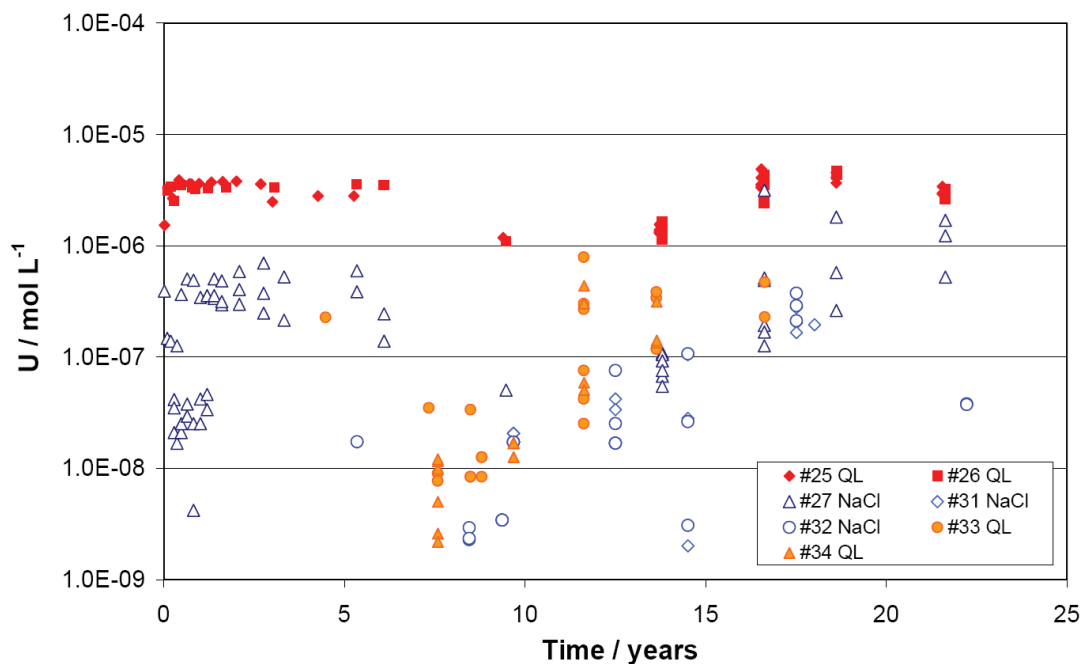


Fig. 7 Observed uranium release from simulated full-scale cemented waste forms [56].

2.9 Wastes solidified in bitumen and plastic materials

Bitumen was used for solidification of nitrate salts from reprocessing and of ion-exchange resin from water treatment in power reactors. Bitumen and plastics as matrices for waste solidification are listed in Tab 5.14 of [3] at a mass of 136 Mg and 49 Mg, respectively.

The behavior and release of radionuclides from bituminized waste forms have been published [61-65]. According to Eschrich [66] the density of bituminized nitrate salts is 1.36 g cm^{-3} , the activity $\sim 1 \text{ Ci m}^{-3}$ ($3.7 \times 10^{10} \text{ Bq dm}^{-3}$). The leach rates of NaNO_3 -containing bitumen waste forms are listed in Tab. 14.

Tab. 14 Leach rates of NaNO_3 containing bitumen waste forms [66]

NaNO_3 content	5 wt. %	10 wt. %	20 wt. %	30 wt. %
mean leach rate / $\text{g cm}^{-2} \text{ d}^{-1}$	4×10^{-6}	7×10^{-6}	2×10^{-5}	9×10^{-5}

Spent ion exchange resins are considered to be waste that in many cases require special treatment and pre-conditioning during its immobilization to meet the acceptance criteria for disposal. A number of processes have been investigated for solidification of the ion-exchange resin, such as solidification in cement, bitumen, organic polymers, urea-formaldehyde, polystyrene-divinylbenzene, thermo-setting resins, and polyethylene [67]. Investigation of adequate plastic materials for solidification of ion-exchange resin are still continuing [68]. Leach rates of spent ion exchange resins solidified in bitumen, cement and plastic material upon exposure to water are shown in Tab. 15.

The solidification of wastes, which contain cation exchanger resins, in a Portland cement matrix was characterized by excessive swelling and cracking of waste forms, both after setting and during immersion testing. High alumina cement formulations displayed a certain resistance to deterioration of mechanical integrity during immersion testing, providing a significant advantage over Portland cements for the solidification of resin wastes.

Tab. 15 Leach rates in water for spent ion exchange resins solidified in various matrices [67]

Matrix	Bitumen	Cement	Polystyrene-divinylbenzene
mean leach rate / $\text{g cm}^{-2} \text{ d}^{-1}$	$10^{-5} - 10^{-4}$	$10^{-3} - 10^{-2}$	$\sim 10^{-3}$

3 Boundary Conditions for the source term

The source term depends strongly on geochemical boundary conditions, which result from the disposal concepts and scenarios. The following Sections compile the relevant data used to derive the geochemical boundary conditions.

3.1 Disposal concept

3.1.1 A – emplacement of wastes with negligible heat generation

Disposal of the wastes with negligible heat generation is regarded in the so-called disposal concept A. Two types of containers were selected [4], which had been developed for the repository for low and intermediate level radioactive wastes “Schacht Konrad”: “Konrad” container type IV and type VI. Type VI is made of >3 mm thick steel plate, while type IV is made of 200 mm armored concrete. Details on the container concept are given in Tab. 16. Note that work package #3 of the vSG project also considers MOSAIK containers or Konrad cast iron container type II as potential disposal casks.

Tab. 16 Dimensions of Konrad containers (box-type) for waste with negligible heat generation [4].

Container type	Konrad type IV (concrete)	Konrad type VI (steel plate)
net weight container [Mg]	9.5 for use of normal concrete, 13.5 for heavy concrete	max 20 incl. waste
length [mm]	3000	1600
width [mm]	1700	2000
height [mm]	1450	1700
volume (outside) [m ³]	7.4	5.4
wall thickness [mm]	200	≥3
volume (inside) [m ³]	3.55	≤ 5.38

The wastes with negligible heat generation are planned to be disposed of in chambers in the west field of the planned repository. According to the optimized concept [69], the chambers in this field will have a cross-section of 41 m² with a distance of 0.1 m between the waste packages. There are planned to be three areas in the west field:

- West1: Uranium tails are planned to be stored in 4 chambers with 1575 containers each + one chamber with 902 containers.

Dividing the inventories by the void volume of each chamber (assuming an initial backfill porosity of 35 %), the resulting concentrations are 12.3 mol/L of U₃O₈ and 7.0×10⁻¹ mol/L of uranyl fluoride UO₂F₂.

Tab. 17 Characteristics of the disposal concept for the uranium tails [3, 4]

container type	Konrad type VI (steel plate)	
chambers	4	1
containers in each chamber	1575	902
chamber characteristics		
length [m]	368	210
volume [m ³]	15068	8629
container volume [m ³]	8568	4907
void volume [m ³]	6500	3722
HM (U ₃ O ₈) [Mg]	24003	13747
uranyl fluoride (UO ₂ F ₂) [Mg]	490	281
residual water [Mg]	120	69
steel (container material)	3630	2079

- West2: Other mixed wastes are planned to be stored in - 11 chambers (~320 m length) with 1068 containers each + one chamber (~226 m length) with 752 containers

Tab. 18 Characteristics of the disposal concept for other mixed wastes [3, 4]

container type	Konrad type IV (armored concrete)	
chambers	8	1
containers in each chamber	1068	831
chamber characteristics		
length [m]	320	249
volume [m ³]	13136	10221
container volume [m ³]	7903	6149
void volume [m ³]	5233	4072
water [Mg]	668	520
concrete (waste/container) [Mg]	170 / 13528	132 / 10526
other inorganics [Mg]	231	179
steel [Mg]	143	111
Al [Mg]	52	41
inorganic carbon compounds [Mg]	52	40
ashes [Mg]	9	7
Zr [Mg]	8.8	6.8
cellulose [Mg]	3.1	2.4
other organic compounds [Mg]	1.4	1.1
others [Mg]	0.18	0.14

Dividing the inventories by the void volume of each chamber (assuming an initial backfill porosity of 35 %) the resulting concentrations of selected exemplary compounds are 1.4 mol/L of Fe from the steel, 1.06 mol/L of Al and 5.0×10^{-3} mol/L of C₁₂H₂₂O₁₁ of cellulose.

- West3: Graphite wastes are planned to be stored in - one chamber (~94m length) with 313 containers

Tab. 19 Characteristics of the disposal concept for the graphite wastes [3, 4]

container type	Konrad type IV (armored concrete)
chambers	1
containers in the chamber	313
chamber characteristics	
length [m]	93.9
volume [m ³]	3850
container volume [m ³]	2316
carbon stone / bricks [Mg]	1540
graphite [Mg]	660
residual water [Mg]	10
concrete (container material) [Mg]	2974*

* assuming the use of containers made of normal concrete

Fig. 8 gives an overview of the west field where the waste with negligible heat generation is planned to be stored.

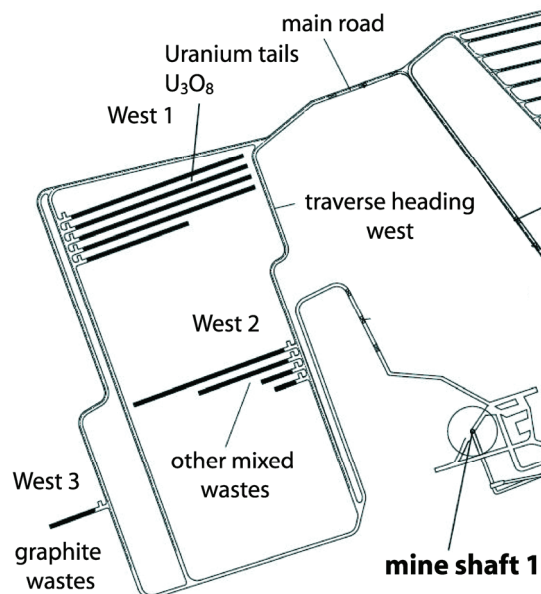


Fig. 8 West field section of the planned repository building (according to the optimized disposal concept of Bollingerfehr [69]).

3.1.2 B1 and B2 - emplacement in horizontal galleries

Disposal in horizontal galleries is considered within disposal concepts B1 and B2 [4]. In both concepts B1 and B2, the waste from research and prototype reactors are planned to be disposed in specially designed CASTOR casks (see Tab. 20). The design of the cask may differ due to the requirement to exclude criticality.

Tab. 20 Dimensions of CASTOR containers for waste of prototype and research reactors [4].

Container	CASTOR AVR/THTR/KNK	CASTOR MTR
max. weight incl. waste [Mg]	26	16
container material	cylindrical body of cast iron with nodular graphite (0.7040); primary lid of cast iron (St 52-3), secondary lid of structural grade carbon steel (TSt E 355)	cylindrical body of cast iron with nodular graphite (0.7040); primary lid of fine grained or stainless steel (1.0566 or 1.4313), secondary lid of fine grained steel (1.0566)
diameter [mm]	1380	1430
length [mm]	2784	1631
volume (outside) [m ³]	4.16	2.62
wall thickness [mm]	390	355
volume (inside) [m ³]	0.57	0.33

Tab. 21 Container concept for wastes from research and prototype reactors [4].

Origin of wastes	Container type	Number of casks	Average no. of fuel elements per cask
AVR	CASTOR AVR	152	1900 spherical fuel elements
THTR	CASTOR THTR	305	2100 spherical fuel elements
KNK II	CASTOR KNK	4	approx. 600 (total 2413 in 4 casks)
NS Otto Hahn			52 in one of the 4 casks
FRM II	CASTOR MTR	20	6 fuel elements
BER II			6 fuel elements

The CASTOR containers with the wastes from the research and prototype reactors will be stored in the east field "Ost 1" of the repository (Fig. 9).

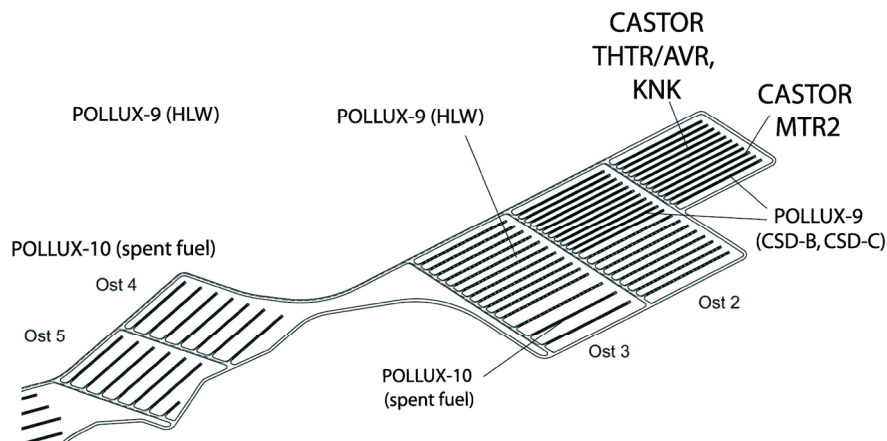


Fig. 9 East field of the planned repository building where wastes from research reactors are planned to be stored (according to disposal concept B1 [4])

According to the present disposal concept the horizontal galleries in the east fields will have a cross-sectional area of 17 m². From the data of the optimized disposal concept [69], an average length of 245 m for the disposal galleries was calculated with an average volume of 4165 m³ and approx. 61 CASTOR AVR/THTR per gallery. With the container geometries given in Tab. 20 and a distance of 1 m between the waste packages this results in a void volume per gallery of approximately 3597 m³. This volume will be backfilled with crushed rock salt having a maximum initial porosity of 35 %. The remaining initial void volume per gallery calculates to 1260 m³. With ongoing time the void volume will decrease due to the compaction of the crushed rock salt.

3.1.3 C - emplacement in vertical boreholes

Disposal in vertical boreholes is considered within disposal concept C [4]. According to this concept, the waste from research and prototype reactors will be disposed in BSK casks or modified BSK casks (see Tab. 22). According to the optimized disposal concept [69], the BSK and modified BSK casks with the wastes from the research and prototype reactors are planned to be stored in 6 vertical boreholes in gallery "Ost 1.2" in the east field of the repository. The boreholes will have a length of ~300 m and a diameter of ~600 mm for the normal BSK casks. The annular gap as well as the uppermost 10 m of the boreholes will be backfilled with crushed salt of 35 % initial porosity.

Tab. 22 Dimensions of BSK casks for waste of prototype and research reactors [4]

Container	BSK	Modified BSK
waste type	KNK & NS Otto Hahn fuel rods in special cases, FRM II, BER II and FRMZ fuel elements	AVR and THTR fuel elements in cans (4 AVR cans or 2 THTR cans)
max. weight incl. waste [Mg]	5.3	< 5.3
container material	cylindrical body, primary and secondary lid of fine grained steel (1.6210); moderator plate underneath primary lid	cylindrical body, primary and secondary lid of fine grained steel (1.6210); moderator plate underneath primary lid
diameter [mm]	430	705
length [mm]	4980	4980
volume (outside) [m³]	0.72	1.94
wall thickness [mm]	40	40
volume (inside) [m³]	~ 0.43	~ 1.38

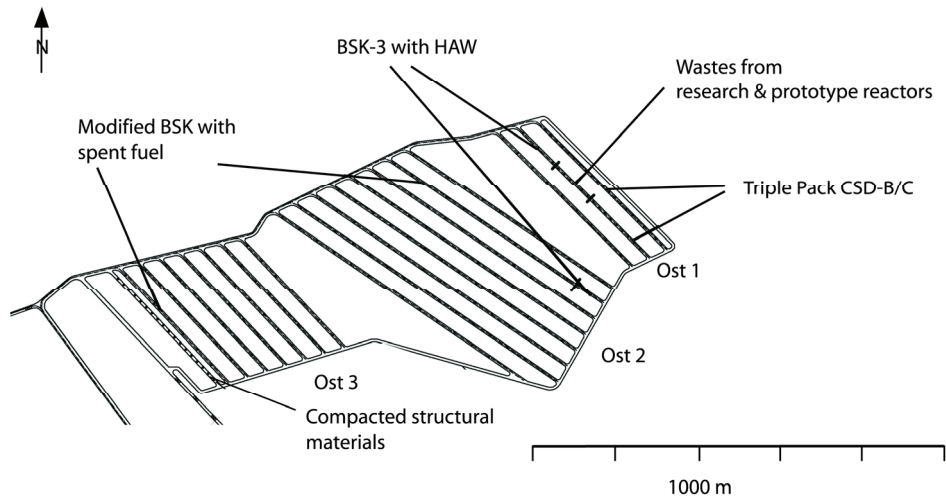


Fig. 10 East field of the planned repository building, where wastes from research reactors are planned to be stored (according to disposal concept C [69])

3.2 Evolution of the geochemical conditions

Information on pH and redox conditions in the emplacement room is indispensable for the determination of the source term. A summary of characteristic data for some emplacement rooms and the specific wastes is shown in Tab. 23. For the wastes in armored concrete containers (Konrad type IV), such as “graphite-wastes from decommissioning” or “other mixed wastes” sufficient amounts of concrete are available in the emplacement rooms for pH buffering by portlandite in a range between 12.0 and 13.0. Geochemical simulations for the $MgCl_2$ - and the $NaCl$ system are shown in Fig. 11 and Fig. 12. Depending on the chamber, the cement to brine ratio (ξ in kg cement per kg water) results between 1.0 and 2.0. In the case of $MgCl_2$ -rich solution entering the chambers, exchange reactions between cement and solution will cause a transformation of solution into $CaCl_2$ -rich solution with pH_m close to 12.0. Experimental results from laboratory experiments with hardened cement paste at ξ between 0.5 and 1.1 as well as results from full-scale experiments at $\xi = 3.0$ with cemented waste simulates are shown for comparison. In the $NaCl$ -rich solution, sodium and chloride concentrations will slightly decrease but still remain high (5.0 - 5.5 mol (kg water)⁻¹) with pH_m values close to 13.0. Results from full-scale experiments with $\xi = 2.8$ are close to the calculated results.

Assessment of the geochemical conditions is much more complicated in the case of the uranium tails. If this material is disposed in steel containers (Konrad type VI), a reducing environment will be achieved due to the anaerobic corrosion of these containers in contact with solution. One can assume that after failure of the steel canisters, the uranium concentration in the disposal room will increase immediately to some 0.7 mol/L due to the UO_2F_2 component of the waste. One may assume that the pH will be controlled by the remaining HF in the tails.

The application of concrete containers for the uranium tails is strongly recommended since it may buffer the pH and Ca would be available to react with fluoride precipitating stable minerals, such as fluorite / CaF_2 of fluorapatite / $Ca_5(F(PO_4)_2)_2$. A similar mechanism of converting UF_6 to the less soluble $UO_2(s)$ by reaction with limestone to form CaF_2 has been proposed by [70]. However, no experimental investigation has been done so far to confirm the transformation under laboratory and repository conditions.

Tab. 23 Characteristic data of some emplacement rooms for specific wastes

	Uranium Tails ^b	Graphite-wastes from decommissioning	Other mixed wastes
No. of emplacement rooms	4 + 1	1	8 + 1
Volume of chambers	15068 m ³	3850 m ³	13136 m ³
No. of canister per chamber	1575 + 902	313 <i>armored</i>	1068 + 831 <i>armored</i>
canister type	steel container Konrad type VI	<i>concrete</i> containers (Konrad type IV)	<i>concrete</i> containers (Konrad type IV)
Canister volume _{tot} per chamber	8568 m ³	2316 m ³	7903 m ³
void volume (without backfill)	6500 m ³	1534 m ³	5233 m ³
Mass of steel	3630 Mg: 27.14 mol/L Fe ^a		
Mass of concrete	<i>alternative ^b: concrete container</i>	3008 Mg	10263 Mg
Mass of cement	<i>alternative ^b: 3384 Mg</i>	673 Mg 8.77 mol/L CaO ^a	2295 Mg 7.02 mol/L CaO ^a
Mass of resins	12.90 Mg		
Mass of others	U ₃ O ₈ : 24003 Mg 35.03 mol/L U ^a UO ₂ F ₂ : 490 Mg 0.66 mol/L U ^a	1540 Mg carbon bricks 660 Mg graphite	
ξ in kg cement/kg water	<i>alternative ^b: 1.5 ≤ ξ_{max} ≤ 2.0</i>	1.3 ≤ ξ _{max} ≤ 1.7	1.0 ≤ ξ _{max} ≤ 1.5
expected pH buffer	<i>alternative ^b: portlandite</i>	portlandite	portlandite

^a In case of complete flooding of the chamber (assuming a backfill porosity of 35 %)

^b In order to buffer the pH and Ca concentration in the vicinity of Uranium Tails, we suggest concrete containers as an alternative to Konrad type IV containers.

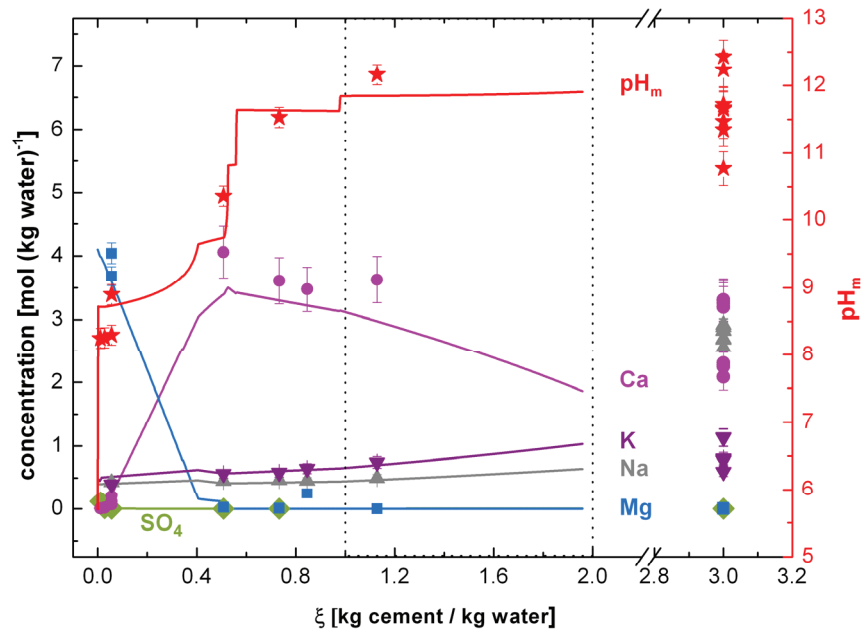


Fig. 11 Evolution of pH_m and major cations in initially MgCl_2 -rich solutions upon reaction with cement product. Lines represent simulated results, symbols represent results from experiments at laboratory-scale in the case of $\xi < 1.1$ and with full-scale cemented waste simulates in the case of $\xi = 3.0$.

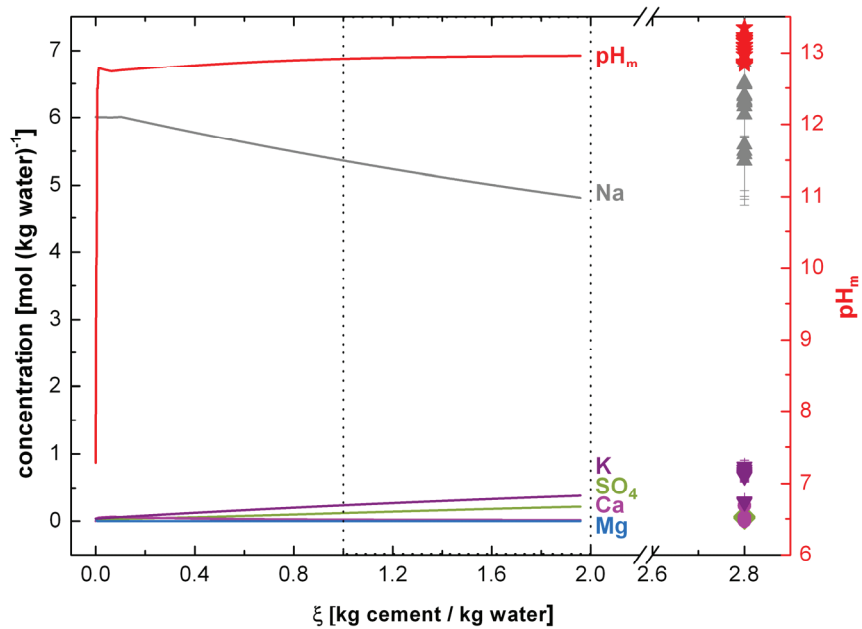


Fig. 12 Evolution of pH_m and major cations in initially NaCl -rich solution upon reaction with cement product. Lines represent simulated results, symbols represent results from experiments with full-scale cemented waste simulates at $\xi = 2.8$.

3.3 Generation of H₂ in a LLW emplacement chamber in the presence of steel containers

Most of the waste with negligible heat generation, such as cemented waste, is packed in steel sheet canisters, cast steel canisters or in self-shielding concrete casks. Specific corrosion rates of these materials are not available under the saline conditions. Therefore, it is referred to canisters of the MOSAIK® type which are produced of cast iron with nodular graphite (GGG40). The iron of these canisters contains recycled low contaminated scrap metal. MOSAIK® II canisters are used for storage and disposal of evaporator concentrates and ionic exchanger resins. Manufacturers are Siempelkamp and GNS.

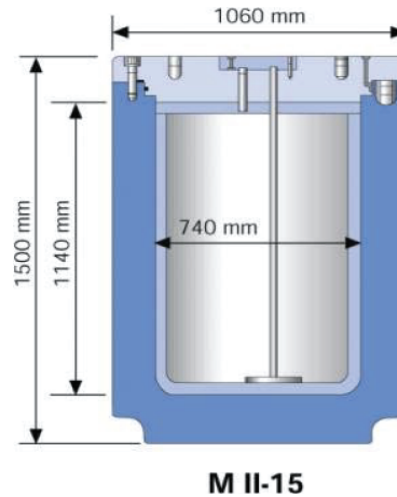


Fig. 13 Schematic illustration of MOSAIK® II canister for disposal of evaporator concentrates and ionic exchanger resins (image provided by GNS)

Mosaik type containers are available also in a cubic shape. The wall thickness is ~160 mm, the weight is between 3 and 10 Mg. The maximal weight the cubic cast iron container is some 20 Mg.

Box type steel plate containers are produced in different sizes mainly for taking compacted waste forms. Konrad IV and VI type containers are considered for the wastes to be disposed of in the West field [4]. While the Konrad IV type canisters will be made of concrete, the Konrad VI type canisters to be used for the Uranium tails will be made of steel plates. The dimensions of these steel plate containers are 1600 × 2000 × 1700 mm³ at a gross volume of 5.4 m³ and a wall thickness of ≥ 3 mm (Tab. 16). Corrosion rates of steel canisters under anaerobic conditions have been determined by Smailos et al. [71-75], Tab. 24. The measured H₂ generation corresponded to that expected from the formation of magnetite.

Tab. 24 Corrosion of nodular graphite steel GGG 40.3 and fine grained steels as function of the temperature in MgCl₂-rich and saturated NaCl solution (after Smailos et al. [71-75]).

T °C	1.0566 in MgCl ₂ -rich solution	TSTE355 in MgCl ₂ -rich solution	GGG 40.3 in MgCl ₂ -rich solution	1.0566 in NaCl solu- tion	TSTE355 in NaCl solu- tion
35		7 µm/yr			9 µm/yr
90	70 µm/yr		50 µm/yr	5 µm/yr	
150	199 µm/yr	160 µm/yr	240 µm/yr	46 µm/yr	40 µm/yr

For an emplacement room with a volume of 15068 m³ filled with 1575 steel canisters, the steel mass is around 3630 Mg. The ratio between mass of steel and brine filled volume amounts to 27.14 mol Fe/L brine. The total exposed steel surface in a flooded chamber is 29 000 m². At a corrosion rate of 10 µm/yr, the total mass loss amounts to 3.6×10⁴ mol Fe forming 4.8×10⁴ mol H₂(g) or 1077 m³ H₂ under normal pressure. This volume is certainly sufficient to establish a H₂ atmosphere in the disposal room within less than one year after flooding. Even if the corrosion rate is only 1 µm/yr, the amount of H₂ gas is still sufficient to establish reducing conditions.

3.4 Chemical degradation processes

In the past, cellulose degradation under alkaline conditions was investigated with respect to its ability of increasing the mobility of cations of the transition metals, the lanthanide and the actinide series [76-78]. Due to degradation, strong complexants are formed, e.g. isosaccharinic acids, 3-deoxy-2-C-hydroxymethyl-D-erythro-pentonic acid (R-ISA) and 3-deoxy-2-C-hydroxymethyl-D-threo-pentonic acid (-ISA).

The time needed for complete degradation of cellulose is important in the context of long-term safety of cementitious repositories for low- and intermediate-level radioactive waste, since large amounts of cellulose may be present. Glaus et al. [77] reports the results of a 12 year study on the degradation of four different cellulosic materials (pure cellulose, tissue, cotton, paper) in artificial cement pore water under anaerobic conditions at ~25° C. The observed reaction characteristics were divided into a fast reaction phase (2-3 years), dominated by a stepwise conversion of terminal glucose monomeric units to α-ISA and β-ISA, and a slow reaction phase during which the same products were found. It was postulated that an unknown mechanism by which crystalline or inaccessible reducing end groups of the polysaccharide chain become temporarily susceptible to alkaline attack were responsible for the slow rate of cellulose degradation. Glaus et al. [77] concluded that "In view of the new data and the model presented here the range of uncertainty for complete degradation of cellulose under repository conditions can be narrowed to a best estimate of 10³ to 5×10³ years".

3.5 Biodegradation processes

The model inventory assumed for the "other wastes with negligible heat generation" contains a large variety of components such as resins, plastics, bitumen, cellulose, and other organic materials, which may be decomposed by microbial activity. It is not clear, if such processes will take place, but various halophilic bacteria isolated at WIPP have the potential to degrade cellulose and other organic materials [79]. The microbial degradation of cellulose and plastic materials was investigated in the context of the US WIPP project [80] and the German ERAM and Asse II sites.

Francis et al. [80] investigated the biodegradation of mixed cellulose (paper, irradiated plastic and rubber materials, e.g. polyethylene, polyvinylchloride, etc.). Microbial gas generation was studied under different conditions:

- starting atmosphere (air or nitrogen)
- humidity (~70 % relative humidity) and presence of brine
- nutrients (nitrogen, phosphate, yeast extract, and excess nitrate)
- potential backfill material (bentonite)

Total gas production was analyzed with respect to CO₂, H₂, N₂, O₂, CH₄, and H₂S. The rate of gas production from cellulose biodegradation in the presence of brine (1228 days at 30 °C) showed an initial rapid rate up to approximately 600 days incubation, followed by a slower rate. More gas was produced in samples containing nutrients, especially excess nitrate, relative to those without a nutrient addition. The total rate of gas production is listed in the report, which has been amended after 10.8 years duration of the experiments [81]. Some results are summarized in Tab. 25.

Tab. 25 Degradation and CO₂ formation by microbial degradation of cellulose [81]

	aerobic conditions g ⁻¹ cellulose	anaerobic conditions g ⁻¹ cellulose
total gas without nutrients	0.84 ± 0.10 ml	2.84 ± 0.31 ml
total gas with nutrients	1.71 ± 1.03 ml	4.12 ± 0.76 ml
total gas with nutrients and nitrate	12.2 ± 0.0 ml	18.1 ± 0.38 ml
CO ₂ formation without nutrients	16.3 ± 1.3 μmol	27.44 ± 5.8 μmol
CO ₂ formation with nutrients	41.4 ± 7.8 μmol	66.9 ± 1.1 μmol
CO ₂ formation with nutrients and nitrate	186 μmol	251 ± 5 μmol
CH ₄ formation without nutrients	1.34 ± 0.03 nmol	5.89 ± 1.30 nmol
CH ₄ formation with nutrients	0.84 ± 0.05 nmol	2.74 ± 0.90 nmol
CH ₄ formation with nutrients and nitrate	1.27 ± 0.37 nmol	2.57 ± 0.79 nmol

Methane was first detected after 7.4 years incubation in brine inundated samples. Cellulose degradation products found in the solutions include fumaric, lactic, oxalic, oxalacetic, propionic, and succinic acids indicating fermentative microbial activity. Microbial gas production of polyethylene or polyvinylchloride samples was not observed after ~7 years incubation. Irradiated rubber materials such as neoprene and hypalon showed a certain CO₂ production.

Microbial degradation of bituminized waste forms also cannot be excluded. Tab. 26 shows the degradation and CO₂ formation rates by microbial attack of bitumen under aerobic and anaerobic conditions.

Tab. 26 Degradation rate and CO₂ formation rate by microbial degradation of bitumen [64, 82]

	Degradation rate g m ⁻² yr ⁻¹	CO ₂ formation rate g m ⁻² yr ⁻¹
aerobic conditions	30 – 35	1 – 1.3
anaerobic conditions	0.2 – 0.6	(0.7 – 2.0) × 10 ⁻²

4 Performance of containers

4.1 Self-shielding concrete waste containers

Self-shielding concrete waste containers are made of a typical concrete composition as given in Tab. 27. Depending on the required degree of shielding, gravel or hematite are used as additives. For investigation of the durability, self-shielded concrete waste containers have been immersed into Q-brine at 40 °C. They were inspected regularly. After 5.5 years, the concrete containers showed the formation of 4 - 5 mm thick layer at their top surfaces. Below this, a 2 mm layer of corroded concrete was detected. The cylindrical walls showed negligible corrosive attack. After 7.3 years, some material had crumbled from the corners. The solution was clear, except for some precipitated $\text{Mg}(\text{OH})_2$ flocks. In general, the concrete containers were in a good condition. Only the cement material that had been used for filling the gaps showed a higher susceptibility to corrosion. After 10.9 years, the experiments were terminated, samples removed from the solution and cut along the cylindrical axis (Fig. 14).

The $[\text{Mg}^{2+}]$ decreased by a factor of almost 2 and $[\text{SO}_4^{2-}]$ by a factor of 4.5 during the leaching period. These concentrations are different from those determined for cemented waste forms. These results indicate a reduced corrosion rate due to the low porous concrete used as shielding material. Cs^+ and the NO_3^- , which were components of the simulated waste form, could not be detected in the solution after 10.9 yr. The progress of corrosion was determined visually and by means of measurements of the pressure resistance (ricochet hardness with a Schmidt hammer). Significant differences were found in those parts of the concrete container filled with poured cement material. Typical findings in the composition of the concrete after ~11 years of storage in MgCl_2 brine are shown in Tab. 28.

In these experiments, the changes of the composition of the corroding Q-brine was less significant than that, found in leaching experiments of cemented waste forms. The porosity of the cylindrical concrete wall was very low. Hence, exchange processes and correlated corrosion did not play a significant role during the corrosion experiments. On the other hand, parts of the lid which had been filled with a rather porous cementitious material as sealing compound showed strong corrosive attack, which would lead to a loss of tightness. Concluding from the measured data, the tightness of a self-shielded concrete waste container is expected to be given only for a period of 30 to 50 years. The durability of the cylindrical concrete walls used as radiation shielding is considerably longer [54].



Fig. 14 Cut through a cylindrical self-shielded concrete disposal container after corrosion in saturated MgCl_2 solution (Q brine) for 11 yrs.

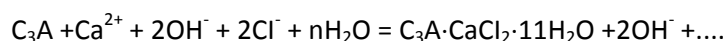
Tab. 27 Initial composition of the concrete.

Concrete class (German)	B35 with steel support
Cement content	370 kg m^{-3}
Plasticizer	2 kg m^{-3}
Water/Cement ratio (W/C)	0.51
Additives	1940 kg m^{-3} gravel or 2940 kg m^{-3} hematite

Tab. 28 Changes in the composition of the concrete after ~11 years storage in MgCl_2 brine

Penetration depth	Observation
0-2.5 cm	strong corrosion fractures (gypsum, sylvinite, sored phases)
2.5-5 cm	grain bonds disturbed (monochloride,...)
5-11 cm	mechanically intact structure
up to 3 cm	penetration of sulfate
up to 5 cm	penetration of Mg^{2+}
> 11 cm	penetration of Cl^-

Chloride interaction with concrete materials has been studied under various conditions and reported in literature. For example, the diffusion was investigated recently [83]. These investigations covered NaCl solutions up to 3 M. Together with penetration of Cl^- into the cement matrix, the formation of Friedels' salt takes place according to the reaction given below (see for example [84-87]).



C_3A : Calcium aluminate hydrate

$\text{C}_3\text{A} \cdot \text{CaCl}_2 \cdot 11\text{H}_2\text{O}$: Friedels' salt

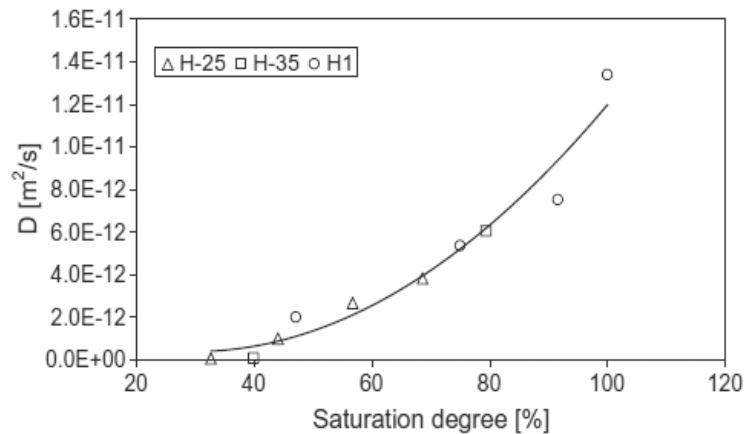


Fig. 15 Chloride diffusion coefficients in cement at different degrees of water saturation [83].

Fig. 15 shows the chloride diffusion coefficients in Portland cement products with different degrees of water saturation. These data have been derived from experimental investigations [83]. Using the diffusion coefficient for saturated concrete and taking into account that the formation of Friedel's salt may reduce the mechanical stability of the containers, a life-time of Konrad type IV containers of 40 - 50 years can be calculated¹. The life-time of the packages could be increased by filling the containers completely without leaving any remaining void volume.

4.2 Steel containers

Data on the corrosion of nodular graphite steel GGG 40.3 and fine grained steels as function of the temperature in $MgCl_2$ -rich solution and saturated NaCl solution are given in chapter 3.3.

For steel plate canisters of a wall thickness ≥ 3 mm, failures may occur if a certain brine pressure is present which exceeds the stability of the containers. Also in this case, a complete backfill of the containers would be beneficial.

¹ penetration of Cl^- into some 10 cm of the wall thickness of the concrete container

5 Source Term

5.1 Kinetics of radionuclide release

Fuel elements from the AVR/THTR

According to Fachinger and Duwe [14] and Zhang [16] the long-term release rate for HEU BISO and LEU TRISO can be estimated to a fraction of $2 \times 10^{-9} \text{ day}^{-1}$. This rate corresponds to a complete dissolution within 1.37 Mio. years.

Fuel elements from the KNK II and NS Otto Hahn

It is reasonable to assume that the kinetics of the radionuclide release from the fuel elements from KNK II and NS Otto Hahn are influenced strongly by the heavily disturbed and fractured appearance of the fuel. After failure of the canisters, the fraction of instantly released radionuclides is estimated to be in the upper range compared to spent fuel from power reactors [1]. Instant release fractions assumed for these fuel elements are shown in Tab. 29.

Tab. 29 Percentage of rapid (instant) radionuclide release from NS OTTO HAHN fuel assuming a heavily disturbed UO_2 matrix.

fission gas	16 %
^{14}C	10 %
^{36}Cl	28 %
^{90}Sr	9 %
^{99}Tc , ^{107}Pd	9 %
^{129}I , ^{135}Cs , ^{137}Cs	16 %

Fuel elements from the research reactors BER II and FRM II

The aluminum matrix of the spent fuel element of BER II and FRM II will be disintegrated instantaneously in salt brines with respect to the time periods relevant for a final repository. The corrosion rate in saturated NaCl is expected to be in the range of $10 \text{ wt. \% year}^{-1}$, in MgCl_2 rich solutions complete corrosion will place within < 20 days. This means that after failure of the canisters, the radionuclides will be instantly released from these materials.

Graphite Wastes

An average mass loss rate was determined in the range of 4.7×10^{-10} to $1.9 \times 10^{-11} \text{ g m}^{-2} \text{ day}^{-1}$ in water at $20 \text{ }^\circ\text{C}$ for French and US reactor graphite over a period of 3 month showing a constant or decreasing rate.

Compacted structural materials from conditioning of spent fuel elements from LWRs

Tanabe [44] differentiates between the radionuclide release from cladding material - in the Japanese reference case as instant release of the oxide film on the zircaloy - and complete dissolution of the metallic matrix within 7600 yrs. For BWR cladding after $39.4 \text{ GWd/t}_{\text{HM}}$, the oxide film amounted to 2.2 wt. % of the zircaloy metal. For the case of a rock salt environment, no data are available.

Tails from uranium enrichment

The UO_2F_2 component in the waste from uranium enrichment is expected to be released very fast as no retention mechanism is known. After failure of the steel canisters, the uranium concentration in the disposal room can immediately reach some 0.7 mol/L corresponding to the complete inventory of the uranyl fluoride compounds.

Other mixed wastes with negligible heat generation

The mixed wastes with negligible heat generation are characterized insufficiently, so that a complete and instantaneous release of the radionuclides needs to be assumed.

Cemented waste forms

Corrosion of cemented waste forms in chloride-rich solutions has been studied in long-term full-scale experiments under in-situ conditions [53, 54] and in laboratory-scale batch experiments [88]. In saturated NaCl solution, the wastes undergo diffusive leaching. Easily soluble compounds including Cs, will be released according to the coefficients given in Tab. 13. In the case of MgCl_2 solutions, cemented waste forms corrode fast and are disintegrated within 15 - 20 years. The disintegration causes an increase of surface area. By this process, the radionuclides are mobilized faster as in the case of NaCl solution. Actinides and lanthanides will be retained if their inventory exceeds their solubility.

5.2 Maximum radionuclide concentrations in the emplacement rooms

The maximum radionuclide concentrations depend on the actual geochemical environment, such as pH and redox properties, complexing ligands and on the solubility controlling solids being stable in the respective environment. In the present study, this geochemical environment can only be assessed for emplacement rooms with well-defined inventories and boundary conditions. The geochemical environment that results from mixing of solutions which have been in contact with the waste forms of different emplacement rooms cannot be characterized currently.

Fuel elements from research and prototype reactors

Fuel elements from the AVR/THTR, KNK II, the MS Otto Hahn and the research reactors BER II and FRM II will be disposed of close to the high-level wastes and spent fuel from power reactors. They are also conditioned in steel canisters. For this reason, the same geochemical boundary conditions and the same solubility controlled elemental concentrations can be applied as reported in [1] in "Tab. XVIII Solubility controlled element concentrations in the relevant pH_m range".

Tails from uranium enrichment

This material is planned to be disposed in steel plate containers (Konrad container type VI) providing for a reducing environment after brine access. Radiolysis is not relevant, because of the relatively low dose rate of the waste product. U_3O_8 in the tails undergo a slow reduction to solid $\text{UO}_2(\text{am})$ which would result in U concentrations below 10^{-6} mol/L at neutral to alkaline pH conditions. However, 2 % of the tails consist of uranyl fluoride UO_2F_2 which can be dissolved completely. Consequently, the maximum concentration of U is inventory controlled with respect to the mass of UO_2F_2 per emplacement room.

Other wastes with negligible heat generation

Graphite wastes, compacted structural materials from conditioning of spent fuel elements from LWRs, cemented waste forms and wastes solidified in bitumen and plastic materials are intended to be packed in armored concrete containers (Konrad container type IV). Depending on the pore volume of the emplacement rooms, a huge mass of concrete (cement) is available and the pH will be controlled by portlandite in the range $12 \leq \text{pH} \leq 13$ (see Tab. 23). In the case of MgCl_2 brine access Ca-Mg exchange reactions with the cement phase may lead to a CaCl_2 dominated solution in the emplacement rooms. Furthermore, sufficient steel is available in the armor, drums and wastes in order to establish reducing redox conditions. Tab. 30 shows the geochemical conditions of NaCl, MgCl_2 and CaCl_2 -rich solution and the dominant radionuclide oxidation states expected in the emplacement rooms containing the wastes with negligible heat generation. The carbonate and sulfate concentrations were calculated using the HMW data base [89].

Tab. 30 Geochemical conditions of NaCl, MgCl_2 and CaCl_2 solution and dominating radionuclide oxidation states expected in the emplacement rooms containing the wastes with negligible heat generation.

Reference system	NaCl system 5.6 m NaCl	MgCl_2 system 4.0 m MgCl_2	CaCl_2 system 2.0 m CaCl_2
Carbonate	calcite saturation: 4×10^{-6} mol/L	calcite saturation: 2×10^{-4} mol/L	calcite saturation: 3×10^{-6} mol/L
Sulfate	Gypsum saturation: 5×10^{-2} mol/L	Gypsum saturation: 2×10^{-2} mol/L	Gypsum saturation: 3×10^{-3} mol/L
pH	$-\log [\text{H}^+] = 12.8$	$-\log [\text{H}^+] = 9$	$-\log [\text{H}^+] = 12$
Redox conditions	reducing	reducing	reducing
Radionuclide oxidation state			
Americium	Am(III)	Am(III)	Am(III)
Thorium	Th(IV)	Th(IV)	Th(IV)
Uranium	U(IV), U(VI)	U(IV), U(VI)	U(IV), U(VI)
Neptunium	Np(IV)	Np(IV)	Np(IV)
Plutonium	Pu (III), Pu(IV)	Pu (III), Pu(IV)	Pu (III), Pu(IV)
Technetium	Tc(IV)	Tc(IV)	Tc(IV)
Zirconium	Zr(IV)	Zr(IV)	Zr(IV)

According to Brendebach [90] and Altmaier [91, 92], in high pH solutions and in the presence of high Ca^{2+} concentrations, actinides form stable positively charged ternary complexes such as $\text{Ca}_3[\text{Zr}(\text{OH})_6]^{4+}$, $\text{Ca}_4[\text{Th}(\text{OH})_8]^{4+}$ or $\text{Ca}_2[\text{Pu}^{\text{III}}(\text{OH})_4]^{3+}$, $\text{Ca}_3[\text{Pu}^{\text{III}}(\text{OH})_6]^{3+}$, and $\text{Ca}_4[\text{Pu}^{\text{IV}}(\text{OH})_8]^{4+}$. These complexes increase the dissolved element concentrations by orders of magnitude. The slope in the increase of concentrations with pH_m 2 for $\text{ZrO}_2 \cdot x\text{H}_2\text{O}(\text{s})$ and 4 in the case of $\text{ThO}_2 \cdot x\text{H}_2\text{O}(\text{s})$ and Plutonium. However, in the presence of solid materials, one may assume that these complexes easily undergo sorption due to their high positive net-charge.

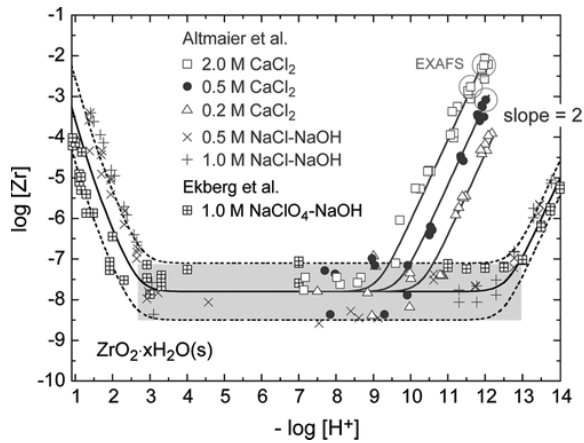


Fig. 16 Solubility of $ZrO_2 \cdot xH_2O(s)$ in $NaClO_4$, $NaCl$, and $CaCl_2$ solutions at 20-25 °C [90].

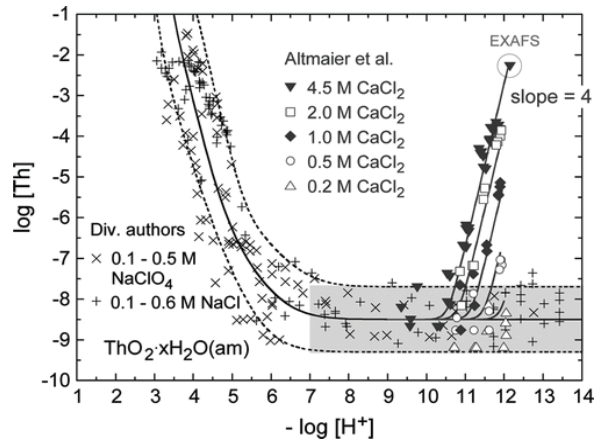


Fig. 17 Solubility of $ThO_2 \cdot xH_2O(s)$ in $NaClO_4$, $NaCl$, and $CaCl_2$ solutions at 17-25 °C [90].

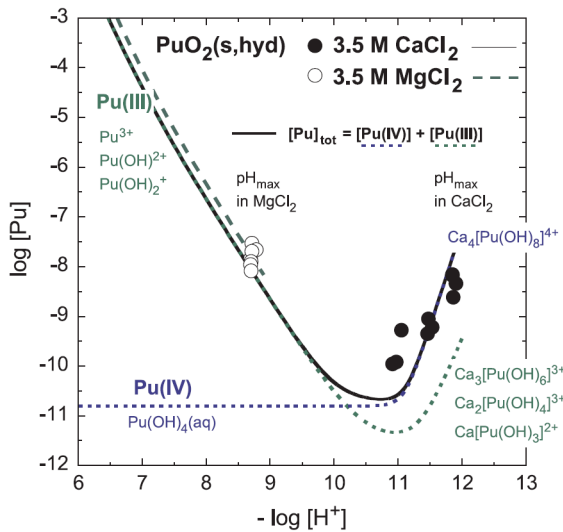


Fig. 18 Solubility of $PuO_2 \cdot xH_2O(s)$ in $MgCl_2$ and $CaCl_2$ solutions [92].

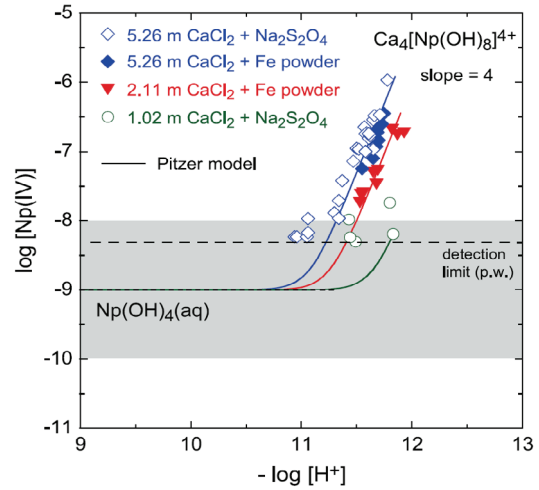


Fig. 19 Solubility of $NpO_2 \cdot xH_2O(s)$ in $CaCl_2$ solutions [93].

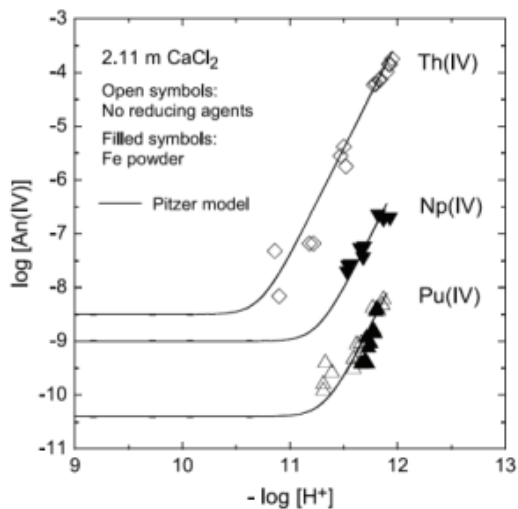


Fig. 20 Comparison of tetravalent actinide solubility in $CaCl_2$ solution [93].

The thermodynamic solubility of tetravalent Zr, Th, Np and Pu is shown in Fig. 16 to Fig. 20. The solubility and the complexation in the high Ca^{2+} solutions is shown for the pH range relevant in the emplacement rooms for wastes with negligible heat generation in armored concrete containers. The solubility controlled element concentrations given in Tab. 31 are relevant for pure radionuclide solution systems without the presence of any sorbing solid.

Tab. 31 Solubility controlled upper-limit concentrations in NaCl, MgCl_2 and CaCl_2 solution for the emplacement rooms of wastes with negligible heat generation (unit: mol L^{-1})

	NaCl system	MgCl_2 system	CaCl_2 system
Am(III)	10^{-7}	$10^{-4.5}$	10^{-6}
Th(IV)	10^{-6}	10^{-6}	$> 10^{-3}$
U(IV)	10^{-6}	10^{-6}	10^{-6}
U(VI)	10^{-6}	$10^{-5.5}$	10^{-6}
Np(IV)	10^{-6}	10^{-6}	10^{-6}
Np(V)	10^{-4}	10^{-3}	10^{-6}
Pu(III)	10^{-7}	10^{-8}	10^{-8}
Pu(IV)	10^{-8}	10^{-8}	10^{-8}
Zr(IV)	10^{-6}	10^{-6}	$> 10^{-2}$
Tc(IV)	10^{-6}	10^{-6}	10^{-6}
Tc(VII)	$> 10^{-1}$	$> 10^{-1}$	$> 10^{-1}$

The total mass of the radioactive elements are low in the wastes with negligible heat generation. Solubility limits are not expected to be reached under the selected disposal conditions. For example, the highest nuclide activities of the wastes with negligible heat generation sums up to the following quantities of radioactive isotopes in 15000 m^3 of waste volume: Tc: 21 mol, I: 6540 mol, Cs: 9 mol, Th: 423000 mol, U: 46600 mol, Pu: 80 mol and Am: 4 mol (re-calculated from [3]).

In the case of the presence of solid materials, sorption processes will take place and change the observed concentrations to lower values under many conditions. As soon as radionuclides are transported away from the source, they certainly will undergo sorption onto surfaces of container corrosion product, backfill material etc., which will decrease their concentrations in the near field and delay the radionuclide transport. It is emphasized, that the given radionuclide concentrations are only relevant for pure solution systems.

The data in Tab. 31 already account for chloride complexation. Other natural complexing components such as CO_3^{2-} or SO_4^{2-} , may affect the maximal actinide concentrations as well. Radionuclide complexes with sulfate SO_4^{2-} are normally weaker in comparison to carbonate complexes. At the sulfate concentrations assumed for the present solutions (cf. Tab. 30) and pH values above 6, uranium complexation with sulfate is negligible compared to hydroxo or carbonato complexes. They may gain relevance at lower pH or in the case of high sulfate concentrations in the solution. The predominance of hydroxo complexes over sulfato and carbonato complexes is shown in Fig. 21 for the NaCl system. For MgCl_2 - and CaCl_2 -rich solutions, adequate thermodynamic models and parameters (Pitzer coefficients) to describe carbonate and sulfate complexation with radionuclides are missing. The concentrations of CO_3^{2-} and SO_4^{2-} ligands relevant for this study are given in Tab. 30.

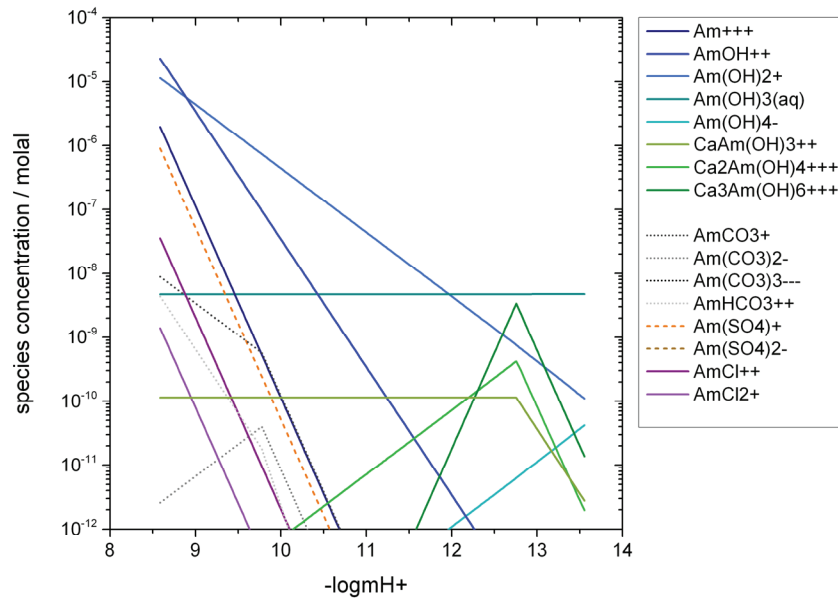


Fig. 21 Speciation diagram of Am in NaCl solution in the presence of CO₃ and SO₄ according to data given in Tab. 30.

5.3 Effect of organic complexing agents

The maximum concentrations of the solubility controlled elements may be influenced by the presence of organic complexing agents. The following compounds of the "other mixed wastes" are relevant in this context: Isosccarinic acid, EDTA, citrate, tartrate, oxalate, and surfactants. Tab. 12 shows the total inventory of these compounds: 27.4 Mg cellulose, 0.28 kg Fe(NH₄)-EDTA and Na₂-EDTA, 250 kg Na₃-citrate, K₃-citrate, Na₂-hydrogen-citrate, (NH₄)₂-hydrogen-citrate, Na₂-tartrate, and Na₂-oxalate citrate, as well as 142 kg anionic, nonionic and cationic surfactants. This inventory is distributed over 12 emplacement rooms resulting in ~24 g EDTA per emplacement chamber. Using the molar mass of EDTA of 292.24 g mol⁻¹, and the void volume of the emplacement chambers (Tab. 23), the EDTA concentration would be ~5×10⁻⁸ mol/L, calculated by dividing the inventory by the void volume of the emplacement chambers. Comparing the inventory of EDTA to that of complexing agents "other than EDTA" (Tab. 12), the concentrations of these non-EDTA compounds would be in the range of ~10⁻⁵ mol/L, which is higher by a factor of 1000. In the context of previous source term projects for Gorleben [94], ERAM [95, 96] and Asse II [97], KIT-INE performed a number of experiments investigating the effect of complexing agents on the solubility and the sorption behavior of RN in near-neutral carbonate free MgCl₂ and NaCl brine systems. The results of these investigations suggest that EDTA is the most efficient complexing agent. The maximum EDTA concentration in the solubility experiments was 1×10⁻³ mol/L.

In [96] the effect of 1×10⁻³ mol/L EDTA on the solubility of U₃O₈(s), PuO₂(s), and ThO₂(s) was evaluated in detail. The measured actinide concentrations were found to be increased by a factor of 5 for U and Pu in the MgCl₂-rich solution, and 20 - 30 in saturated NaCl solution. For Th, dissolved concentrations were found to be increased by a factor of 172 in MgCl₂ brine and 480 in NaCl solution. However, this high increase could not be related to the effect of EDTA, because in these experiments a decrease of the pH by more than two units was observed. As can be seen in Fig. 16 ff., such a pH decrease can lead to solubility increase by several orders of magnitude.

Within a project on determining the solubilities of radionuclides under Asse II specific conditions [97], the maximum concentrations for Th, Np, U, Pu and Nd were measured both from undersaturation (in contact with a representative solid) and from oversaturation. All measurements were performed in MgCl_2 -rich solution at a $\text{pH}_m \sim 9$. The solutions have been obtained by equilibrating Q-brine with typical constituents of the disposal rooms, e.g. with the dominant macroscopic near-field components. The measured actinide concentrations in presence of 1×10^{-3} mol/L EDTA were found to be increased by a factor of 22 for Pu, 42 for Nd(III), 6 for Np(V), 3 for U(VI) and 11 for Th(IV). At concentrations of 1×10^{-4} mol/L EDTA, the effect was negligible. The same is true for the complexing agents "other than EDTA".

According to Glaus [77], a significant part of the cellulose could be degraded to iso-saccharinic acid only after several hundred years. Extrapolating linearly the degradation rate given by Glaus [77] (Fig. 4), tissues will degrade at a rate of < 0.001 per year. The sorption of ISA on cement reduces the concentration of ISA in the pore water to $\sim 10^{-4}$ M [98].

Overall, the amount of complexing agent present in the wastes seems to be too low to significantly influence radionuclide concentrations. In addition, the availability of organic ligands is limited by interaction with the major solution components, e.g. Ca^{2+} . This is not valid for the uranium tails under the present disposal concepts, since, in this case, the large amount of fluorides will affect the uranium concentrations.

6 Sorption

6.1 Sorption onto zircaloy compounds

Sorption onto zircaloy compounds has been investigated [99-101]. Most of the recent publications report sorption site densities and maximum sorption site saturation for hydrous ZrO_2 . The sorption site density for UO_2^{2+} sorption on the hydrous oxides of Zr and Th was determined in the range of 1 to 2.5 sites nm^{-2} [102].

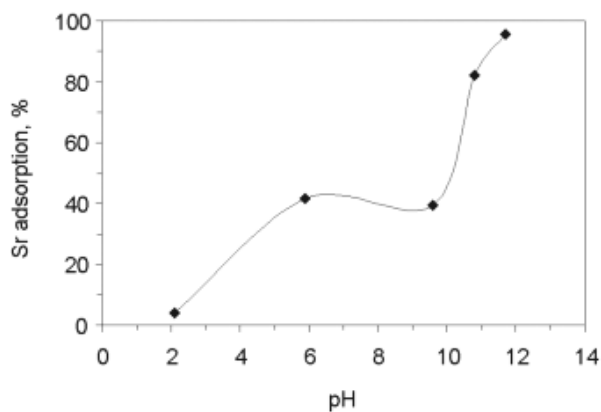


Fig. 22 Effect of pH on the sorption behavior of Sr onto hydrous ZrO_2 [100].

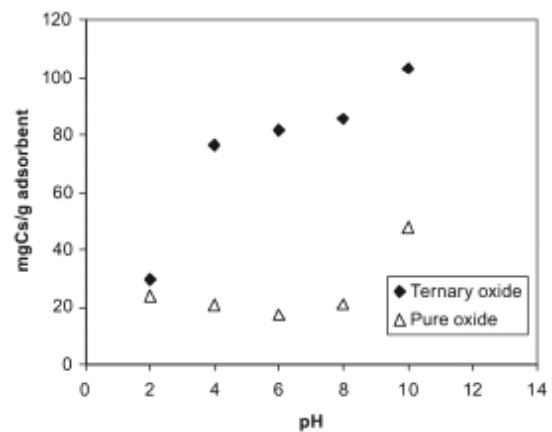


Fig. 23 Effect of pH on the sorption behavior of Cs onto hydrous ZrO_2 [99] (at pH = 10: 20 % adsorption)

However, sorption onto corroded zircaloy can hardly be considered as a significant retention barrier for radionuclides.

6.2 Sorption onto iron phases

Sorption of some radionuclides onto different iron oxides/hydroxides have been published in literature, however, very few data are reported for concentrated salt solutions. An overview is given in the following table. Many of these publications cover the interaction mechanisms or derive surface complexation model (SCM) constants.

Most of the data reported in Tab. 32 can be applied only to specific geochemical conditions (pH, ionic strength). The retention processes of the cationic elements onto the iron phases, e.g. sorption, precipitation, surface complexation, are significant at elevated pH values.

Tab. 32 Overview on sorption experiments for radionuclides onto iron phases

Element	Substrate	Rs / ml g ⁻¹	Citation
U ^{VI}	Magnetite		[103-106]
U ^{VI}	green rust		[107]
U ^{VI}	pyrite		[108]
U ^{VI}	magnetite	3000 @ pH = 8	[109]
Se ^{VI}	green rust, magnetite		[110]
Np ^V	green rust, magnetite		[111], [112]
Th ^{IV}	magnetite, ferrihydrite		[113, 114]
Pu ^{IV}	goethite		[115]
Pu ^{III}	magnetite, mackinawite, chukanovite		[116]
Yb ^{III} , Ni ^{II} , Cs ^I	magnetite	SCM data	[117]
Cs ^I ,	magnetite	18 @ pH = 8	[118]
Sr ^{II} ,		20 @ pH = 8	
Co ^{II}		65 @ pH = 8	
Sr ^{II}	magnetite		[119]
Cs ^I	magnetite	100 @ pH = 10	[120]

6.3 Sorption onto corroded cement products

In the scope of the investigations for ERAM [95] and Asse II [121] sorption on cement systems was studied. The results are listed in the following tables (Tab. 33 - Tab. 35).

Tab. 33 Sorption coefficients (Rs) in the cement/MgCl₂ brine system after about 9 months

Element*	Rs / ml/g		
	without EDTA	0.1 mM EDTA	1 mM EDTA
Am	7710 - 3615	800 - 317	300 - 132
Np	1673 - 1026	1577 - 1008	1693 - 1217
Pu	4767 - 3860	5153 - 3830	3196 - 2273
Ra	20 - 7	31 - 11	15 - 7
Tc	18 - 10	23 - 3	15 - 3
U	8943 - 4840	6310 - 3817	4140 - 2233

* redox states not determined

For the actinides Am and Pu, sorption experiments were performed on corroded cement systems at high pH and high Ca²⁺ concentrations [88]. The experiments aimed on investigating actinide retention under Asse II specific conditions. The solid was CEM I 32,5R with a water to cement ratio W/C = 0.4. The hardened cement paste was powdered and pre-corroded in MgCl₂ solution, Q- and R-brines. Within 3.5 years, Ca / Mg exchange reactions between cement and solution took place and the reaction equilibrium was reached. The effect of different MgCl₂-rich initial solutions on the compositions of solids and solution was not significant. In fact, final concentration of Mg²⁺ and Ca²⁺ in the solutions depended on the solid to brine ratio of the experiments. Model calculations corroborated the measured equilibrium data. Sorption experiments were performed in contact with

two solutions of different Ca^{2+} concentrations and pH values (so-called solutions 3 m Ca and 4 m Ca) representing equilibrated solutions at two different solid to brine ratios. The results (Tab. 34) reveal that significant retention occurs onto the completely corroded cement products, which is relevant in the case of MgCl_2 solution penetrating into the emplacement rooms with cemented wastes.

Tab. 34 Americium and Plutonium retention in high pH and Ca^{2+} systems [88]

Solution (composition)	Am	Pu
3mCa (2.75 m CaCl_2 , 1.55 m MgCl_2)	$R_s = 3100 \pm 1100 \text{ mL g}^{-1}$	measured concentration at/below detection limit $5 \times 10^{-12} \text{ mol (kg H}_2\text{O)}^{-1}$
4mCa (4.0 m CaCl_2)	$R_s = 12800 \pm 7700 \text{ mL g}^{-1}$	measured concentration at/below detection limit $5 \times 10^{-12} \text{ mol (kg H}_2\text{O)}^{-1}$

As can be seen in Fig. 16 ff., high Ca concentrations may lead to an increase in Am concentrations at alkaline pH values. The results in Tab. 34 show that, if sufficient solid (corroded) cement material is present, even in concentrated CaCl_2 solutions total actinide concentrations are controlled by sorption and the effect of increasing actinide solubility concentrations by formation of $\text{Ca}_2[\text{Am}^{\text{III}}(\text{OH})_4]^{3+}$, $\text{Ca}_3[\text{Am}^{\text{III}}(\text{OH})_6]^{3+}$ or $\text{Ca}_2[\text{Pu}^{\text{III}}(\text{OH})_4]^{3+}$, $\text{Ca}_3[\text{Pu}^{\text{III}}(\text{OH})_6]^{3+}$, and $\text{Ca}_4[\text{Pu}^{\text{IV}}(\text{OH})_8]^{4+}$ is not relevant.

Sorption of ^{14}C carbonate was determined onto salt concrete („Salzbeton“) at pH = 10.6 and onto sored concrete at pH 9 in NaCl and in MgCl_2 solutions. A strong dependence on the experimental duration was observed. Sorption coefficients for both solids were found in the range of $R_s \sim 3000 \text{ ml g}^{-1}$ [95] in NaCl solution and significantly lower, $R_s \sim 2$ to 11 ml g^{-1} , in MgCl_2 -solutions. Values measured for the NaCl systems are in good agreement with published data [122-125].

6.4 Sorption onto rock salt

Few data exist on sorption of radionuclides onto solid rock salt. Some results were obtained by INE and are listed partly in [1]. In Tab. 35, sorption coefficients are listed that cover different concentrations of organic complexing agents present in the wastes with negligible heat generation. A size fraction of rock salt between 0.6 and 0.9 mm was chosen. The salt had a low carbon content $C_{\text{total}} \sim 0.023 \pm 0.004 \text{ wt. \%}$ [95].

Tab. 35 Sorption coefficients (R_s) in the systems rock salt (ERAM) / MgCl_2 and NaCl solution [95]

Solution	Elements*	R_s after 280 days / ml/g				
		without EDTA	EDTA 0.01mM	EDTA 0.1mM	EDTA 1mM	Citric acid 1mM
MgCl_2 solution	Pu	20	16	5.9	2.5	3.8
	Th	135	28	5.4	3.4	7.3
	Np	0.2			0.3	0.3
	U	0.4			0.5	0.7
NaCl solution	Pu	301	27	2.5	0.3	1.6
	Th	85	4.9	0.3		1.6
	Np	71			11	2.7
	U					0.2

* redox states not determined

7 Open Questions and Recommendations

Source terms for various waste forms have been derived. Waste forms under investigation are spent fuel elements from the pilot reactors AVR/THTR, from the research reactors KNK II and NS Otto Hahn, as well as from BER II and FRM II. Furthermore, graphite wastes, compacted structural materials from conditioning of spent fuel elements from LWRs and the tails from uranium enrichment are considered. Specific details are provided for other mixed wastes with negligible heat generation, such as cemented waste forms and wastes solidified in bitumen and plastic materials. For these materials, the characteristic physical and chemical properties, element and radionuclide inventory, and the kinetics of radionuclide release are described. The boundary conditions are discussed for several disposal concepts: A - emplacement of wastes with negligible heat generation, B1 and B2 - emplacement in horizontal galleries, and C - emplacement in vertical boreholes. The boundary conditions include the description of the geochemical conditions and the generation of the H₂ atmosphere in LLW emplacement rooms in the presence of steel containers. The geochemical performance of containers of the Konrad type IV and VI is evaluated including self-shielded concrete and steel containers.

The source terms cover the kinetics of radionuclide release and the maximum radionuclide concentrations in the different emplacement rooms under the prevailing geochemical environment. Sorption processes are described for zircaloy compounds, iron phases, corroded cement products and rock salt. Open questions are derived from the compilation of the relevant data and processes of the various waste forms.

- In the wastes with negligible heat generation, a lot of different components may affect the radionuclide concentrations, such as fluorides, artificial complexing agents and some waste degradation products (iso-saccharinic acid). Even if the expected low radionuclide concentrations limit the importance of such complexes for mobilization, the understanding of the relevant processes needs to be developed.
- The spatial distance between the high level waste disposal fields and the disposal fields for wastes with negligible heat generation needs to be sufficiently large. If the temperature of the HAW field affects the wastes with negligible heat generation, the performance of these materials cannot be predicted. For these waste forms, few investigations have been performed and mainly up to 40 °C. Even fewer experimental data exist for higher temperatures.
- Radionuclide retention by sorption processes are described for some relevant materials. However, the sorption database under saline conditions is poor.
- The potential microbial interactions with waste forms, container materials, etc. are not investigated. The effect of degradation of the disposed materials including organics and metals by microbial processes is not known.

Recommendation:

There is a wide variety of different components in the waste forms. Due to the complexity of the different waste components, it is highly recommended to keep the different waste materials separated, especially from the high level waste disposal site.

8 References

- [1] Kienzler, B., M. Altmaier, C. Bube, and V. Metz (2012), Radionuclide source term for HLW glass, spent nuclear fuel, and compacted hulls and end pieces (CSD-C waste), *Vorläufige Sicherheitsanalyse Gorleben (vSG): KIT-SR 7624*.
- [2] Closs, K.D., K. Duphorn, and K. Kühn (2002), Ein- oder Mehr-Endlager-Konzept? . *ATW - Internationale Zeitschrift für Kernenergie* **47**: 302-06
- [3] Peiffer, F., B. McStocker, et al. (2011), Abfallspezifikation und Mengengerüst - Bericht für Arbeitspaket 3, Stand: Juli 2011, in *Vorläufige Sicherheitsanalyse für den Standort Gorleben*, GRS, Editor. GRS, ISTec, nse.
- [4] Bollingerfehr, W., W. Filbert, C. Lerch, and M. Tholen (2011), Enlagerkonzepte für die VSG (Arbeitspaket 5), Stand: Juli 2011, in *Vorläufige Sicherheitsanalyse für den Standort Gorleben*, GRS, Editor. DBE-TEC.
- [5] Brähler, G., M. Hartung, et al. (2012), Improvements in the fabrication of HTR fuel elements. *Nuclear Engineering and Design* **251** (0): 239-243.
- [6] Plätzer, S. and M. Mielisch (1998), Unloading of the reactor core and spent fuel management of the THTR 300, in *Technical committee meeting on technologies for gas cooled reactor decommissioning, fuel storage and waste disposal* International Atomic Energy Agency: Juelich (Germany) 8-10 Sep 1997. p. 143-150.
- [7] Cleve, U. (2011), Die Technologie des Hochtemperaturreaktors und Nukleare Hochtemperaturtechnik zur Erzeugung flüssiger Brennstoffe, von Wasserstoff und elektrischer Energie. *ATW - Internationale Zeitschrift für Kernenergie* **56** (6): 344-353.
- [8] Hackstein, K.-G. and M. Wimmers (1989), Brennstoff-Zyklus, in *AVR- 20 Jahre Betrieb: Ein deutscher Beitrag zu einer zukunftsweisenden Energietechnik*, V.D. Ingenieure, Editor. VDI-Verlag: Düsseldorf. p. 103-114.
- [9] Ivens, G. and M. Wimmers (1989), Der AVR als Testbett für Brennelemente, in *AVR- 20 Jahre Betrieb: Ein deutscher Beitrag zu einer zukunftsweisenden Energietechnik*, V.D. Ingenieure, Editor. VDI-Verlag: Düsseldorf. p. 161-175.
- [10] Fütterer, M.A., G. Berg, et al. (2008), Results of AVR fuel pebble irradiation at increased temperature and burn-up in the HFR Petten. *Nuclear Engineering and Design* **238** (11): 2877-2885.
- [11] Niephaus, D., S. Storch, and S. Halaszovich (1997), Experience with the interim storage of spent HTR fuel elements and a view to necessary measures for the final disposal, in *Technologies for gas cooled reactor decommissioning, fuel storage and waste disposal*. IAEA, Vienna: IAEA-TECDOC--1043.
- [12] IAEA (2006), Characterization, Treatment and Conditioning of Radioactive Graphite from Decommissioning of Nuclear Reactors. International Atomic Energy Agency, Vienna: IAEA-TECDOC--1521.
- [13] Fachinger, J., W. von Lensa, and T. Podruhzina (2008), Decontamination of nuclear graphite. *Nuclear Engineering and Design* **238** (11): 3086-3091.
- [14] Fachinger, J.B., H.; Duwe, R. (1997), R&D intermediate storage and final disposal of spent HTR fuel, in *Technologies for gas cooled reactor decommissioning, fuel storage and waste disposal*. IAEA, Vienna: IAEA-TECDOC--1043.
- [15] Rainer, H. and J. Fachinger (1998), Studies on the long-term behaviour of HTR fuel elements in highly concentrated repository-relevant brines. *Radiochimica Acta* **80**: 139-145.

- [16] Zhang, Z.X. (1993), Study for establishing proof of the long-term safety of ultimate disposal of spent HTR fuel elements in an underground repository embedded in rock strata. Forschungszentrum Juelich GmbH (Germany). Inst. fuer Chemische Technologie.: Juel-2796.
- [17] Pokrovskii, V.A. and H.C. Helgeson (1995), Thermodynamic properties of aqueous species and the solubilities of minerals at high pressures and temperatures: The system Al₂O₃-H₂O-NaCl. *American Journal of Science* **295** (10): 1255-1342.
- [18] Frost, B.R.T. (1982). Nuclear Fuel Elements: Design, Fabrication and Performance. Oxford, Pergamon Press.
- [19] Marth, W. (1993), Die Geschichte von Bau und Betrieb des deutschen Schnellbrüter-Kernkraftwerks KNK II. Kernforschungszentrum Karlsruhe Karlsruhe KfK 5155.
- [20] Wehmann, U., K.H. Wenk, and P. Dünner (1983). Schnellbrüter - Brennelemente. The Fast Breeder Fuel Cycle - Fuel Elements and their Reprocessing, Karlsruhe Kernforschungszentrum 1-20.
- [21] Bleyl, H.J. (1983). Erfahrung mit der Aufarbeitung von KNK-Brennstoff in der MILLI. The Fast Breeder Fuel Cycle - Fuel Elements and their Reprocessing, Karlsruhe Kernforschungszentrum 123-132.
- [22] Kleykamp, H. (1983). Zur derzeitigen Kenntnis über die Zusammensetzung und den chemischen Zustand von Rückständen bestrahlter SBR-Brennstoffen nach Auflösung in Salpetersäure. The Fast Breeder Fuel Cycle - Fuel Elements and their Reprocessing, Karlsruhe Kernforschungszentrum 101-108.
- [23] EUREGIO N/S Otto Hahn - Technische Daten und Einzelheiten. Available from: <http://www.philatel.net/Otto-Hahn/data.html>.
- [24] GKSS (1981), NS OTTO HAHN - Erstes deutsches Kernergieschiff. GKSS-Forschungszentrum Geesthacht GmbH, Geesthacht: GKSS 81/E/20.
- [25] Rogan, P., G. Žerovnik, et al. (2005), Evaluation of zero power experiments with second core of FDR (Advanced Pressurized Light Water Reactor) for the Nuclear Research Ship »Otto Hahn«, in *International Conference "Nuclear Energy for New Europe 2005"*: Bled, Slovenia, September 5-8, 2005.
- [26] Wiese, H.W. (1983). Vergleich berechneter und routinemäßig gemessener Inventare bestrahlter KNK II/1 Brennelemente sowie Berechnung verglasungsrelevanter Spaltstoffe. The Fast Breeder Fuel Cycle - Fuel Elements and their Reprocessing, Karlsruhe Kernforschungszentrum 110-121.
- [27] BMU (2008), Joint Convention on the Safety of Spent Fuel Management and on the Safety of Radioactive Waste Management Report of the Federal Republic of Germany for the Third Review Meeting in May 2009. Federal Ministry for the Environment, Nature Conservation and Nuclear Safety (BMU), Berlin.
- [28] TU Munich (2011), FRMII - The Neutron Source - Brief Description. <http://www.frm2.tum.de/en/technik/brief-description/index.html>.
- [29] Axmann, A. and H.-J. Didier (1993), Ausbau und Betrieb des BER-II. *Atomwirtschaft* **38** (1): 42-47.
- [30] Helmholtz Zentrum Berlin (2012), Forschungsreaktor BERII. http://www.helmholtz-berlin.de/zentrum/grossgeraete/ber2/index_de.html.
- [31] Fachinger, J. and H. Curtius (2000), Long term behavior of direct disposed MTR fuel elements in saline brines, in *Applied Mineralogy in Research, Economy, Technology, Ecology and Culture* Rammlmair, Editor. Balkema: Rotterdam. p. 531-534.
- [32] Curtius, H. and J. Fachinger (2000), Adsorption of radionuclides on aluminium oxide in a repository-relevant brine, in *Applied Mineralogy in Research, Economy, Technology, Ecology and Culture*, Rammlmair, Editor. Balkema: Rotterdam. p. 503-506.
- [33] Rammlmair, D., J. Mederer, et al., Eds. (2000). Applied Mineralogy in Research, Economy, Technology, Ecology and Culture - Volume 2. Rotterdam, Balkema.

- [34] NDA Stakeholder Newsletter (2010), Key graphite study assists disposal. <http://www.nda.gov.uk/stakeholders/newsletter/graphite-study.cfm>.
- [35] Gray, W.J. and W.C. Morgan (1988), Leaching of ^{14}C and ^{36}Cl from Hanford reactor graphite. Pacific Northwest Laboratory, Richland, USA: PNL- 6769.
- [36] Gray, W.J. and W.C. Morgan (1989), Leaching of ^{14}C and ^{36}Cl from irradiated French graphite. Pacific Northwest Laboratory, Richland, USA: PNL- 6989.
- [37] Podrzhina, T. (2004), Graphite as radioactive waste: corrosion behaviour under final repository conditions and thermal treatment. RWTH Aachen, Aachen.
- [38] Willax, H.-O. (1998), Status of the Gorleben Pilot Conditioning Plant. *Nuclear Technology* **121** (2): 128-135.
- [39] Baier, J., R. Jung, and J. Korzeczek (1999). Conditioning of spent fuel for direct disposal - Experiences during cold commissioning of the Pilot Conditioning Plant Gorleben/Germany (PKA). Waste Management'99, Tucson, AZ, February 28 - March 4, 1999, 28 - MARCH 4, 1999.
- [40] Lahr, H., H.-O. Willax, and H. Spilker (1998). Conditioning of spent fuel for interim and final storage in the Pilot Conditioning Plant (PKA) at Gorleben. International Symposium on Storage of Spent Fuel from Power Reactors, Vienna, Austria, 9-13 November 1998, IAEA, **IAEA-SM-352**.
- [41] Neeb, K.-H. (1997). The radiochemistry of nuclear power plants with light water reactors. Berlin, de Gruyter.
- [42] Kupfer, A. (2000), Radiochemische Korrosionsuntersuchungen an Urandioxid und Cladding-Materialien von Kernbrennstoffen in praxisrelevanten Salzlaugen als Beitrag zur direkten Endlagerung. Freie Universität Berlin, Berlin.
- [43] HKL Technology (2003), Investigating zirconium hydride formation in nuclear fuel cladding. Available from: <http://www.hkltechnology.com/data/0-zirconium-hydride.pdf>.
- [44] Tanabe, H. (2007), Characterization of hull waste in underground condition, in *International Workshop on Mobile Fission and Activation Products in Nuclear Waste Disposal (MoFAP)*: L'Hermitage, La Baule, France, January 16-19.
- [45] Johnson, L., C. Poinssot, C. Ferry, and P. Lovera (2004), Estimates of the Instant Release Fraction for UO₂ and MOX Fuel at t=0, in *TR 04-08*, NAGRA, Editor, Wettingen, Switzerland.
- [46] Yamaguchi, I., S. Tanuma, et al. (1999). A study on chemical forms and migration behaviour of radionuclides in hull wastes. ICEM '99, Nagoya, Japan, Sept. 26-30, 1999, ASME.
- [47] URENCO (2006), Enriching the future, U.D. GmbH, Editor.
- [48] Glaus, M.A. and L.R.v. Loon (2004), A generic procedure for the assessment of the effect of concrete admixtures on the retention behaviour of cement for radionuclides: concept and case studies. Nuclear Energy and safety research department: Laboratory for Waste Management, Paul Scherrer Institut, Villigen CH: PSI-Bericht Nr. 04-02.
- [49] Verein deutscher Zementwerke (1984). Zement Taschenbuch. Wiesbaden - Berlin, Bauverlag.
- [50] Biczok, I. (1968). Betonkorrosion, Betonschutz, Bauverlag GmbH, Wiesbaden - Berlin.
- [51] Vejmelka, P., G. Rudolph, W. Kluger, and R. Köster (1990), Die Konditionierung radioaktiver Abfallösungen durch Zementierung. Forschungszentrum Karlsruhe: KfK 4800.
- [52] Vejmelka, P., G. Rudolph, and W. Kluger (1991), Investigations of low and medium-level cemented waste forms from reprocessing Task 3 Characterization of radioactive waste forms A series of final reports (1985-89), No. 4. Nuclear Science and Technology: EUR 13544.
- [53] Kienzler, B., V. Metz, and A. Bauer (2008). Interactions of cemented waste forms with salt brines: Results after 25 years full-scale tests. 5th International Seminar on Radioactive Waste Products (RADWAP 2008), Würzburg, Germany, 27 - 31 October, Forschungszentrum Jülich.
- [54] Kienzler, B., P. Vejmelka, et al. (2000), Long-term leaching experiments fo full-scale cemented waste forms: Experiments and modeling. *Nuclear Technology* **129**: 101-118.

- [55] Kienzler, B. and V. Metz (2009). Modelling long-term corrosion of cemented waste forms in salt brines. 12th Internat. Conf. on Environmental Remediation and Radioactive Waste Management (ICEM '09), Liverpool, GB, October 11-15.
- [56] Kienzler, B., M. Schlieker, et al. (2004), Langzeit Auslaug- und Korrosionsexperimente an zementierten 1:1 Gebinden in der Schachtanlage Asse: Probennahme und Auswertung 2003. Forschungszentrum Karlsruhe: FZKA 7059.
- [57] Lide, D.R. and H.P.R. Frederiske, Eds. (1997). CRC Handbook of Chemistry and Physics, 77th Edition. Boca Raton, New York, London, Tokyo, CRC Press Inc.
- [58] Jakob, A., F.A. Sarott, and P. Spieler (1999), Diffusion and sorption on hardened cement pastes -experiments and modelling results: PSI Report No. 99-05.
- [59] Bube, C., V. Metz, et al. (2011). Interactions of U(VI) with cement alteration products in highly saline solutions. NUWCEM 2011, 1st International Symposium on Cement-based Materials for Nuclear Wastes, Avignon (France).
- [60] Kienzler, B., V. Metz, et al. (2010), Chemical status of U(VI) in cemented waste forms under saline conditions. *Radiochimica Acta* **98** (9-11): 675-684.
- [61] Kluger, W., H. Krause, and O. Nentwich (1969), Fixing of radioactive residues in bitumen Gesellschaft für Kernforschung GmbH, Karlsruhe: KfK-1037
- [62] Flambard, A.R., C. Keiling, H.U. Fusban, and G. Marx (1986), Die Auslaugung von Actiniden und Spaltprodukten aus in Zement und Bitumen verfestigtem ILW und deren Mobilität durch natürliches Steinsalz., J.I. Kim and E. Warnecke, Editors. Physikalisch Technische Bundesanstalt, Braunschweig: SE-34.
- [63] Libert, M.F., R. Sellier, et al. (1993). Effects of micoorganisms growth on the long-term stability of cement and bitumen. *Mat. Res. Soc. Symp.*, **294**, 267-272.
- [64] Wolf, M. (1989), Mikrobieller Abbau von Bitumen.: NAGRA TB 89-14.
- [65] Kluger, W., W. Hild, et al. (1980), Bituminierung radioaktiver Abfallkonzentrate aus Wiederaufarbeitung, Kernforschungseinrichtungen und Kernkraftwerken: KfK 2975.
- [66] Eschrich, H. (1980), Properties and long-term behaviour of bitumen and radioactive waste bitumen mixtures. Svensk Kärnbränslehantering AB (SKB), Stockholm, Sweden: SKBF/KBS TR 80-14.
- [67] IAEA (1981), MANAGEMENT OP SPENT ION-EXCHANGE RESINS PROM NUCLEAR POWER PLANTS. International Atomic Energy Agency (IAEA), Vienna: IAEA-TECDOC-238.
- [68] Roth, A., F. Willmann, et al. (2008). Solidification of radioactive liquid wastes. A comparison of treatment options for spent resins and concentrates. Managment of radioactive wastes, and non-radioactive wastes from nuclear facilities, Avignon (France), 28 Sep - 2 Oct 2008, Societe Francaise d'Energie Nucleaire (SFEN).
- [69] Bollingerfehr, W., S. Dörr, et al. (2012), Enlagerauslegung und -optimierung (Arbeitspaket 6), Stand: Juni 2012, in *Vorläufige Sicherheitsanalyse für den Standort Gorleben*, GRS, Editor. DBE-TEC.
- [70] Laverov, N.P., V.I. Velichkin, et al. (2010), Geological conditions of safe long-term storage and disposal of depleted uranium hexafluoride. *Geology of Ore Deposits* **52**: 261-266.
- [71] Smailos, E., R. Köster, and W. Schwarzkopf (1983), Korrosionsuntersuchungen an Verpackungsmaterialien für Hochaktive Abfälle. *European Appl. Res. Rept. - Nucl. Sci. Technol.* **5** (2): 175-222.
- [72] Smailos, E., W. Scharzkopf, and R. Köster (1987), Corrosion Behaviour of Container Materials for the Disposal of High-Level Waste Forms in Rock Salt Formations: KfK 4265.
- [73] Smailos, E., W. Schwarzkopf , B. Kienzler, and K. R. (1992). Corrosion of Carbon-Steel Containers for Heat-Generating Nuclear Waste in Brine Environments Relevant for a Rock-Salt Repository. Scientific Basis for Nuclear Waste Management: Proc.of the 15th Internat.Symp., Strasbourg, November 4-7, 1991, Materials Research Soc., **257**, 399-406.

- [74] Smailos, E. (1993), Corrosion of high-level waste packaging materials in disposal relevant brines. *Nuclear Technology* **104**: 343-350.
- [75] Smailos, E., A. Martínez-Esparza, et al. (1999), Corrosion evaluation of metallic materials for long-lived HLW/spent fuel disposal containers. Forschungszentrum Karlsruhe: FZKA 6285.
- [76] Glaus, M.A., L.R. Van Loon, et al. (2008), Long-term predictions of the concentration of alpha-isosaccharinic acid in cement pore water. *Scientific Basis for Nuclear Waste Management XXXI* **1107**: 605-612.
- [77] Glaus, M.A. and L.R. Van Loon (2008), Degradation of cellulose under alkaline conditions: New insights from a 12 years degradation study. *Environmental Science & Technology* **42** (8): 2906-2911.
- [78] Glaus, M.A. and L.R. Van Loon (2009), Chemical reactivity of α -isosaccharine acid in heterogeneous alkaline systems. Paul Scherer Institut, Villigen, CH: PSI Bericht Nr. 08-01.
- [79] Vreeland, R.H., A.F. Piselli Jr, S. McDonnough, and S.S. Meyers (1998), Distribution and diversity of halophilic bacteria in a subsurface salt formation. *Extremophiles* **2** (3): 321-331.
- [80] Francis, A.J., J.B. Gillow, and M.R. Giles (1997), Microbial gas generation under expected Waste Isolation Pilot Plant repository conditions. Sandia National Laboratories (ANL), Albuquerque, NM, USA: SAND96-2582.
- [81] Gillow, J.B. and A.J. Francis (2006), Microbial gas generation under expected Waste Isolation Pilot Plant repository conditions: Final report. Brookhaven National Laboratory, Upton, NY, USA: BNL-96148-2011-IR.
- [82] Aalto, H. and M. Valkiainen (1997). Characterization of Bituminized Ion-Exchange Resins for Final Disposal at TVO Power Plant. RADWAP'97, Würzburg.
- [83] Guimarães, A.T.C., M.A. Climent, et al. (2011), Determination of chloride diffusivity through partially saturated Portland cement concrete by a simplified procedure. *Construction and Building Materials* **25** (2): 785-790.
- [84] Chatterji, S. (1994), Transportation of ions through cement based materials. Part 2. Adaptation of the fundamental equations and relevant comments. *Cement and Concrete Research* **24** (6): 1010-1014.
- [85] Birnin-Yauri, U.A. and F.P. Glasser (1998), Friedel's salt, $\text{Ca}_2\text{Al}(\text{OH})_6(\text{Cl},\text{OH})\cdot 2\text{H}_2\text{O}$: its solid solutions and their role in chloride binding. *Cement and Concrete Research* **28** (12): 1713-1723.
- [86] Suryavanshi, A.K. and R. Narayan Swamy (1996), Stability of Friedel's salt in carbonated concrete structural elements. *Cement and Concrete Research* **26** (5): 729-741.
- [87] Cau Dit Coumes, C. and S. Courtois (2003), Cementation of a low-level radioactive waste of complex chemistry: Investigation of the combined action of borate, chloride, sulfate and phosphate on cement hydration using response surface methodology. *Cement and Concrete Research* **33** (3): 305-316.
- [88] Metz, V., E. Bohnert, B. Kienzler, and K. Garbev (2011), Studie zur Abschätzung der standortspezifischen Pu- und Am-Rückhaltung (Schachanlage Asse II): Abschlussbericht Experimentelle Überprüfung der Abschätzung kammer-spezifischer Pu- und Am-Konzentrationen für die Schachanlage Asse II.
- [89] Harvie, C.E., N. Moller, and J.H. Weare (1984), The prediction of mineral solubilities in natural waters: The Na-K-Mg-Ca-H-Cl-SO₄-OH-HCO₃-CO₃-CO₂-H₂O system to high ionic strengths at 25°C. *Geochimica and Cosmochimica Acta* **48**: 723-751.
- [90] Brendebach, B., M. Altmaier, et al. (2007), EXAFS study of aqueous Zr(IV) and Th(IV) complexes in alkaline CaCl₂ solutions: $\text{Ca}_3[\text{Zr}(\text{OH})_6]^{4+}$ and $\text{Ca}_4[\text{Th}(\text{OH})_8]^{4+}$. *Inorganic Chemistry* **46** (16): 6804-6810.
- [91] Altmaier, M., V. Neck, and T. Fanghänel (2008), Solubility of Zr(IV), Th(IV) and Pu(IV) hydrous oxides in CaCl₂ solutions and the formation of ternary Ca-M(IV)-OH complexes. *Radiochimica Acta* **96** (9-11): 541-550.

- [92] Altmaier, M., V. Neck, J. Lutzenkirchen, and T. Fanghänel (2009), Solubility of plutonium in MgCl_2 and CaCl_2 solutions in contact with metallic iron. *Radiochimica Acta* **97** (4-5): 187-192.
- [93] Fellhauer, D., V. Neck, et al. (2010), Solubility of tetravalent actinides in alkaline CaCl_2 solutions and formation of $\text{Ca}_4[\text{An}(\text{OH})_8]^{4+}$ complexes: A study of Np(IV) and Pu(IV) under reducing conditions and the systematic trend in the An(IV) series. *Radiochimica Acta* **98** (9-11): 541-548.
- [94] Kienzler, B., W. Schüßler, and V. Metz (2001), Quellterme für HAW-Glas, abgebrannten Kernbrennstoff und zementierte Abfälle: Berechnung der maximalen Radionuklidkonzentrationen im geochemischen Milieu des Nahfeldes der Abfälle., in *Erstellung eines integrierten Nahfeldmodells von Gebinden hochaktiver Abfälle im Salzstock Gorleben: geochemisch fundierter Quellterm für HAW-Glas, abgebrannte Brennelemente und Zement*. Institut für Nukleare Entsorgung (INE), Forschungszentrum Karlsruhe, Karlsruhe: FZK-INE 002/00.
- [95] Gompper, K. and P. Vejmelka (1998), Nuklidmigration im Deckgebirge des Endlagers für radioaktive Abfälle Morsleben (ERAM). Teil 1: Sorption im Grubengebäude. p. FZK-INE 20/98.
- [96] Kienzler, B. and V. Metz (2001), Bewertung der Reaktionen von Actiniden mit den organischen Komplexbildnern EDTA und Citrat aus den Abfallprodukten in ERAM. Forschungszentrum, Karlsruhe: FZK-INE 009/00.
- [97] Schüßler, W., P. Vejmelka, et al. (2003), Teil 2: Elementlöslichkeiten unter standortspezifischen Bedingungen, in *Experimentelles Programm zur Bestätigung der Ergebnisse von standortspezifischen Modellrechnungen für die Schachtanlage Asse*. FZK-INE, Karlsruhe: FZK-INE 008/03.
- [98] Van Loon, L.R., M.A. Glaus, S. Stallone, and A. Laube (1998), Alkaline degradation of cellulose: Estimation of the concentration of isosaccharinic acid in cement pore water. *Scientific Basis for Nuclear Waste Management Xxi* **506**: 1009-1010.
- [99] Tel, H., Y. Altas, F. Gur, and A. Ugur (2010), Sorption kinetics of cesium on ZrO_2 and ZrO_2 - SiO_2 - TiO_2 microspheres. *Radiochimica Acta* **98** (4): 215-219.
- [100] Inan, S., H. Tel, and Y. Altas (2006), Sorption studies of strontium on hydrous zirconium dioxide. *Journal of Radioanalytical and Nuclear Chemistry* **267** (3): 615-621.
- [101] Lomenech, C., R. Drot, and E. Simoni (2003), Speciation of uranium(VI) at the solid/solution interface: sorption modeling on zirconium silicate and zirconium oxide. *Radiochimica Acta* **91** (8): 453-461.
- [102] Mahal, H.S., B. Venkataramani, and K.S. Venkateswarlu (1981), Sorption properties of oxides VIII: Sorption of uranium on hydrous oxides. *Journal of Inorganic and Nuclear Chemistry* **43** (12): 3335-3342.
- [103] Grambow, B., E. Smailos, et al. (1996), Sorption and reduction of uranium(VI) on iron corrosion products under reducing saline conditions. *Radiochimica Acta* **74**: 149-154.
- [104] Scott, T.B., G.C. Allen, P.J. Heard, and M.G. Randell (2005), Reduction of U(VI) to U(IV) on the surface of magnetite. *Geochimica et Cosmochimica Acta* **69** (24): 5639-5646.
- [105] Rovira, M., S. El Aamrani, et al. (2007), Interaction of uranium with in situ anoxically generated magnetite on steel. *Journal of Hazardous Materials* **147** (3): 726-731.
- [106] El Aamrani, S., J. Gimenez, et al. (2007), A spectroscopic study of uranium(VI) interaction with magnetite. *Applied Surface Science* **253** (21): 8794-8797.
- [107] O'Loughlin, E.J., S.D. Kelly, et al. (2003), Reduction of uranium (VI) by mixed iron (II)/iron (III) hydroxide (green rust): formation of UO_2 nanoparticles. *Environmental Science & Technology* **37** (4): 721-727.
- [108] Scott, T.B., O.R. Tort, and G.C. Allen (2007), Aqueous uptake of uranium onto pyrite surfaces; reactivity of fresh versus weathered material. *Geochimica et Cosmochimica Acta* **71** (21): 5044-5053.

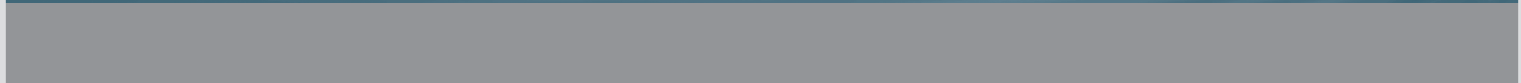
- [109] Missana, T., M. Garcia-Gutierrez, and V. Fernandez (2003), Uranium(VI) sorption on colloidal magnetite under anoxic environment: Experimental study and surface complexation modelling. *Geochimica et Cosmochimica Acta* **67** (14): 2543-2550.
- [110] Puranen, A., M. Jonsson, R. Dähn, and D. Cui (2009), Immobilization of selenate by iron in aqueous solution under anoxic conditions and the influence of uranyl. *Journal of Nuclear Materials* **392** (3): 519-524.
- [111] Christiansen, B.C., H. Geckeis, et al. (2011), Neptunyl (NpO_2^+) interaction with green rust, $\text{GR}(\text{Na}_2\text{SO}_4)$. *Geochimica et Cosmochimica Acta* **75** (5): 1216-1226.
- [112] Nakata, K., S. Nagasaki, et al. (2004), Reduction rate of neptunium(V) in heterogeneous solutions with magnetite. *Radiochim. Acta* **92**: 145-149.
- [113] Rojo, I., F. Seco, et al. (2009), Thorium sorption onto magnetite and ferrihydrite in acidic conditions. *Journal of Nuclear Materials* **385** (2): 474-478.
- [114] Seco, F., C. Hennig, et al. (2009), Sorption of Th(IV) onto Iron Corrosion Products: EXAFS Study. *Environmental Science & Technology* **43** (8): 2825-2830.
- [115] Felmy, A.R., D.A. Moore, et al. (2011), Heterogeneous Reduction of PuO_2 with Fe(II): Importance of the Fe(III) Reaction Product. *Environmental Science & Technology* **45** (9): 3952-3958.
- [116] Kirsch, R., D. Fellhauer, et al. (2011), Oxidation State and Local Structure of Plutonium Reacted with Magnetite, Mackinawite, and Chukanovite. *Environmental Science & Technology* **45** (17): 7267-7274.
- [117] Marmier, N., A. Delisee, and F. Fromage (1999), Surface complexation modeling of Yb(III), Ni(II), and Cs(I) sorption on magnetite. *Journal of Colloid and Interface Science* **211** (1): 54-60.
- [118] Ebner, A.D., J.A. Ritter, and J.D. Navratil (2001), Adsorption of cesium, strontium, and cobalt ions on magnetite and a magnetite-silica composite. *Ind. Eng. Chem. Res.* **40** (7): 1615-1623.
- [119] de Pablo, J., M. Rovira, et al. (2008), Magnetite sorption capacity for strontium as a function of pH. *Scientific Basis for Nuclear Waste Management XXXI* **1107**: 593-598.
- [120] Granizo, N. and T. Missana (2006), Mechanisms of cesium sorption onto magnetite. *Radiochim. Acta* **94**: 671-677.
- [121] Lützenkirchen, J., P. Vejmelka, V. Metz, and B. Kienzler (2003). Site specific sorption data for the Asse salt mine. The 9th International Conference on Radioactive Waste Management and Environmental Remediation ICEM '03, Oxford, England, September 21 – 25.
- [122] Dayal, R. and E.J. Reardon (1994), Carbon-14 behaviour in a cement-dominated environment: Impacts for spent Candu resin waste disposal. *Waste Management* **14** (5): 457-466.
- [123] Dayal, R. and E.J. Reardon (1994), Cement-based engineered barriers for carbon-14 isolation. *Waste Management* **12**: 189-200.
- [124] Noshita, K., T. Nishi, M. Matsuda, and T. Izumida (1996). Sorption of carbon-14 by hardened cement paste. *Mat. Res. Soc. Proc.*, **412**, 435-442.
- [125] Noshita, K., T. Nishi, M. Matsuda, and T. Izumida (1996). Sorption mechanism of carbon-14 by hardened cement paste. *Mat. Res. Soc. Symp. Proc.*, **412**, 435-442.

Annex A Abbreviations

AGR:	advanced gas cooled reactor (UK)
AP:	work package
AVR:	Arbeitsgemeinschaft Versuchsreaktor GmbH, high-temperature research reactor at research centre Jülich
BER:	research reactor Berlin
BISO:	pyro carbon coated fuel particle (Bistructural ISOtropic)
BSK:	disposal canister for spent fuel
BWR:	boiling water reactor
D_a :	apparent diffusion constant
D_w :	diffusion constant for a tracer in pure water
CASTOR:	transport and storage cask for spent fuel
CSD-C:	Colis Standard des Déchets Compactés: Compacted hulls, end pieces and spacers
DTA:	differential thermal analyses
EDTA:	ethylenediaminetetraacetic acid (artificial complexing agent)
EXAFS:	X-ray Absorption Spectroscopy (XAS) includes both Extended X-Ray Absorption Fine Structure (EXAFS) and X-ray Absorption Near Edge Structure (XANES).
FE:	Fuel element
FIMA:	burn-up in fissions per initial metal atom
FRJ:	research reactor Jülich
FRM:	research reactor Munich
FZJ:	research centre Jülich
GfK:	Gesellschaft für Kernforschung Karlsruhe mbH, today Karlsruhe Institute of Technology (Campus North)
GKSS:	research centre Geesthacht
GNS:	Gesellschaft für Nuklear Service mbH
HEU:	highly enriched uranium: According to the American Society of Standards and Testing materials (ASTM) HEU is any uranium with a ^{235}U assay of more than 20 %. Fresh research reactor fuel has ^{235}U assays ranging from below 20 % to as high as 93 % ^{235}U .
ILW:	intermediate level waste
KfK:	research centre Karlsruhe, today Karlsruhe Institute of Technology (Campus North)
Konrad type IV container:	20'' disposal container for activated components with negligible heat generation
KNK:	Karlsruhe sodium cooled reactor
LEU:	low enriched uranium (^{235}U assay of less than 20 %)
LLW:	low level waste

Abbreviations

LWR:	light water reactor
M5:	cladding material (fuel rods)
MAGNOX:	CO ₂ cooled, graphite moderated reactors using natural uranium in Magnox alloy cladding
MCNP:	Monte Carlo N-particle transport code developed by Los Alamos National Lab
MOSAIK:	disposal canister for activated components with negligible heat generation
MTR:	material test reactor
NS:	nuclear ship "Otto Hahn"
pH _m :	-log [H ⁺]
PKA:	pilot conditioning plant at Gorleben
PWR:	pressure water reactor
POLLUX:	disposal canister for spent fuel
PSI:	Paul Scherer Institute, Switzerland
PyC:	pyrocarbon
SEM-EDX:	scanning electron microscope with energy dispersive spectrometry
SUR:	Siemens education reactor
THTR:	thorium high temperature reactor
TLK:	dry storage can (designed for AVR fuel elements)
TRISO:	coated fuel particle (TRistructural ISOtropic)
TRIGA:	reactor for training, research, isotope productions, developed by General Atomics
V/m:	volume to mass ratio in sorption studies
VBA:	concrete shielding disposal cask for insertion of 200 or 400 l drums
W/C:	water to cement ratio for cement and concrete production
XRF:	X-ray fluorescence analysis
XRD:	X-ray diffraction analysis
Zyr:	Zircaloy, zirconium alloy used for cladding material
ξ:	indicator for the reaction progress in geochemical calculations



ISBN 978-3-86644-964-0

